2

High Resolution Measurements of Strained Diffusion and Reaction Layer Structure and Extinction in Turbulent Flows

WERNER J.A. DAHM

AFOSR 89-0541

Annual Report
Period Ending October 31, 1990

GAS DYNAMICS LABORATORIES
of the
DEPARTMENT OF AEROSPACE ENGINEERING
THE UNIVERSITY OF MICHIGAN
Ann Arbor, Michigan 48109-2140

2

High Resolution Measurements of Strained Diffusion and Reaction Layer Structure and Extinction in Turbulent Flows

WERNER J.A. DAHM

AFOSR 89-0541

Annual Report
Period Ending October 31, 1990

GAS DYNAMICS LABORATORIES
of the
DEPARTMENT OF AEROSPACE ENGINEERING
THE UNIVERSITY OF MICHIGAN
Ann Arbor, Michigan 48109-2140

REPORT DOCUMENTATION PAGE

Form Approved
OMB No. 0704-0188

1. AGENCY USE ONLY (Leave blank)	2. REPORT DATE	3. REPORT TYPE AND DATES COVERED
		ANNUAL Rpt 1 - 31Aug90

4. TITLE AND SUBTITLE

High Resolution Measurements of Strained Diffusion Layer Structure and Extinction in Turbulent Flows

5. FUNDING NUMBERS

PE - 61102F
PR - 2308
TA - A2
G - 89-0541

6. AUTHOR(S)

W. J. A. Dahm

7. PERFORMING ORGANIZATION NAME(S) AND ADDRESS(ES)

Gas Dynamics Laboratories
Department of Aerospace Engineering (2140)
The University of Michigan
Ann Arbor MI 48109-2140

8. PERFORMING ORGANIZATION REPORT NUMBER

9. SPONSORING/MONITORING AGENCY NAME(S) AND ADDRESS(ES)

AFOSR/NA
Building 410
Bolling AFB DC 20332-6448

10. SPONSORING/MONITORING AGENCY REPORT NUMBER

11. SUPPLEMENTARY NOTES

12a. DISTRIBUTION/AVAILABILITY STATEMENT

Approved for public release; distribution is unlimited

12b. DISTRIBUTION CODE

13. ABSTRACT *(Maximum 200 words)*

Work on development and use of new, high-resolution, four-dimensional, quantitative imaging measurements of the fully space and time varying fine scale structure of turbulent reacting flows has achieved several important milestones. Our development of this imaging diagnostic capability for turbulent flows was successfully accomplished and has been accepted for publication in a *Springer Verlag* volume (Dahm, Southerland & Buch 1990). Results from our use of this novel diagnostic in experiments documenting the detailed fine scale structure of mixing and reactions in turbulent flows have been presented (Dahm, Southerland & Buch, 1990) and submitted for publication in *Physics of Fluids A* (Dahm, Southerland & Buch 1990). These results directly show that virtually all of the molecular mixing occurs isolated and interacting strained laminar diffusion layers with a self-similar internal structure. A study of the interaction between the fluid strain field and the dynamics of these molecular diffusion layers has also been accepted for publication in *Physics of Fluids A* (Southerland, Porter, Dahm & Buch 1991). A major result is the identification of the diffusional cancellation process between adjacent interacting layers. This work has also resulted in a new method for detailed whole-field velocity measurements in this flow using a unique scalar imaging velocimetry (SIV) technique developed under our effort. We have also examined an apparent similarity in the fine scale structure of turbulent flows seen from our four-dimensional imaging measurements and the "lamellar microstructure" seen in recent experiments on mixing in low Reynolds number chaotic flows. Early results from this joint work undertaken with J.M. Ottino suggest a remarkable degree of universality in the fine structure of mixing, which appears to span across the boundaries of the Reynolds number regimes traditionally associated with such low Reynolds number chaotic flows and with fully turbulent flows.

14. SUBJECT TERMS	15. NUMBER OF PAGES
Turbulent flows, Mixing, Turbulent Reacting Flows, Turbulent Combustion, Turbulent Flames	16. PRICE CODE

17. SECURITY CLASSIFICATION OF REPORT	18. SECURITY CLASSIFICATION OF THIS PAGE	19. SECURITY CLASSIFICATION OF ABSTRACT	20. LIMITATION OF ABSTRACT
Unclassified	Unclassified	Unclassified	UL

GAS DYNAMICS LABORATORIES
of the
DEPARTMENT OF AEROSPACE ENGINEERING
THE UNIVERSITY OF MICHIGAN
Ann Arbor, Michigan 48109-2140

High Resolution Measurements of Strained Diffusion and Reaction Layer Structure and Extinction in Turbulent Flows

AFOSR Grant No. 89-0541

Annual Report
for the Period Ending
31 October 1990

Werner J.A. Dahm
Gas Dynamics Laboratories
Department of Aerospace Engineering
The University of Michigan
Ann Arbor, MI 48109

Executive Abstract

Our work on the development and use of new, high-resolution, four-dimensional, quantitative imaging measurements of the fully space and time varying fine scale structure of turbulent reacting flows has achieved several important milestones which are summarized in this Report. Our development of the first fully-resolved, four-dimensional, quantitative, imaging diagnostic capability for turbulent flows was successfully accomplished and is described in a manuscript accepted for publication in a *Springer Verlag* volume of new laser techniques in fluid dynamics (Dahm, Southerland & Buch 1990). Results from our use of this novel diagnostic in a first set of experiments documenting the fully detailed fine scale structure of mixing and reactions in turbulent flows have also been presented at a specialists meeting (Dahm, Southerland & Buch, 1990) and have been submitted for publication in *Physics of Fluids A* (Dahm, Southerland & Buch 1990). These results directly show that essentially all of the molecular mixing occurs isolated and interacting strained laminar diffusion layers with a self-similar internal structure. A study of the interaction between the fluid strain field and the dynamics of these molecular diffusion layers in the carefully controllable flow field offered by the laminar vortex ring has also been accepted for publication in *Physics of Fluids A* (Southerland, Porter, Dahm & Buch 1991). A major result of this work is the identification of the diffusional cancellation process between adjacent interacting layers. This work has also resulted in a new method for detailed whole-field velocity measurements in this flow using a unique scalar imaging velocimetry (SIV) technique developed under our effort. The successful development of a new local integral model which incorporates these experimental results to allow approximate yet accurate and fast simulations of the mixing and complex chemical reaction processes in turbulent flows has also been accepted for publication in *Combustion & Flame* (Tryggvason & Dahm 1991). This work, which also involves support from the Gas Research Institute, has led to a further manuscript detailing its application for simulating the complex nonlinear phenomena, including local extinction, associated with large Zel'dovich number Arrhenius kinetics in a shear layer. This work has been presented at a specialists meeting (Chang, Dahm & Tryggvason 1990) and has been submitted for publication in *Physics of Fluids A* (Chang, Dahm & Tryggvason 1990). We have also begun to examine an apparent similarity in the fine scale structure of turbulent flows seen from our four-dimensional imaging measurements and the "lamellar microstructure" seen in recent experiments on mixing in low Reynolds number chaotic flows. Early results from this joint work undertaken with J.M. Ottino suggest a remarkable degree of universality in the fine structure of mixing, which appears to span across the boundaries of the Reynolds number regimes traditionally associated with such low Reynolds number chaotic flows and with fully turbulent flows.

Table of Contents

1.0 Introduction and Overview

This research program represents a combined experimental and theoretical effort with the following three major objectives:

(i) to develop high-resolution, multi-dimensional, quantitative, imaging diagnostic capabilities for obtaining direct experimental measurements of the fine scale structure associated with the molecular mixing and chemical reaction processes in turbulent flows,

(ii) to use this measurement technique to experimentally determine the physical characteristics of the fine structure associated with molecular mixing and chemical reactions in turbulent flows, and

(iii) to incorporate results from these measurements into an improved understanding of the molecular mixing, chemical reaction, and local extinction processes in reacting turbulent flows.

The current program addresses the fully space and time varying fine scale structure of $Sc \gg 1$ scalar mixing in turbulent flows with a unique four-dimensional, high-resolution, non-intrusive imaging technique developed as part of this effort. In parallel with this, highly resolved imaging measurements of $Sc \approx 1$ scalar mixing in gaseous turbulent flows are also being conducted. The principal feature is that in both cases the highly resolved nature of the measurements, together with their very high signal quality, permit direct differentiation of the data to allow accurate evaluation of the derivatives in the scalar gradient field involved in forming the scalar energy dissipation rate per unit mass. The resulting simultaneous conserved scalar and scalar dissipation fields permit highly detailed analysis of the structure and reaction progress in finite rate chemically reacting turbulent flows for which the instantaneous thermochemical state of the reacting flow is a unique function of the instantaneous conserved scalar and scalar dissipation fields. In this context, the present highly resolved and multi-dimensional measurements of the conserved scalar field fine structure provide a previously inaccessible means for directly determining many detailed features of mixing and chemical reaction processes in turbulent flows, including the local extinction of reactions in strained diffusion layers and the resulting global combustion stability characteristics of reactive turbulent flows.

1.1 Background

Molecular mixing in turbulent flows plays a central role in an enormous range of practical problems, ranging from the reacting flow processes occurring in future hypersonic airbreathing propulsion systems to the reduction of environmental pollutants in virtually all practical combustion systems. Many such problems can be formulated, either

directly or in certain limiting cases, in terms of the mixing of a dynamically passive conserved scalar quantity. This refers to any scalar property that is advected by the fluid and diffuses relative to the fluid, but which is neither created nor destroyed within the flow and which does not directly affect the flow field. Relevant examples include the concentration field in the mixing of two different inert gaseous streams, the atomic mixture fraction in chemically reacting turbulent flows, as well as numerous others. Sometimes the diffusivity D of the quantity being mixed is comparable to the vorticity diffusivity ν of the fluid; in other words the Schmidt number $Sc \equiv (\nu/D)$ is approximately unity. However, in many other cases the diffusivity of the scalar property can be much smaller than that of the vorticity, so that $Sc \gg 1$. In many problems of this type, and especially those in which some sort of reaction or phase change is involved, it is processes occurring at the fine structure level of the scalar field that can be crucially important in determining the outcome of the mixing. Indeed, the fine structure of passive scalar mixing in non-reacting turbulent flows is a subject of inherently wide interest, since in many important practical situations it allows a direct evaluation of the thermochemical state and reaction progress in an equivalent reactive turbulent flow.

It was recognized not long after the introduction of Kolmogorov's (1941) universal similarity hypotheses that some aspects of this theory also applied to the fine structure of dynamically passive scalar fields being mixed in high Reynolds number turbulent flows. The subsequent modifications to Kolmogorov's original hypothesis of a homogeneous statistical distribution of the dissipation, introduced to account for the spatial 'spottiness' of the vorticity and kinetic energy dissipation, have their parallels in the scalar field fine structure. In particular, Batchelor (1959) recognized that, when the scalar diffusivity D is significantly smaller than the vorticity diffusivity ν, the essentially uniform strain rate ε over regions in the flow much smaller than the finest vortical lengthscale λ_ν provides a mechanism for sustaining scalar gradients over lengthscales $\lambda_D \ll \lambda_\nu$. In that case, the limiting scale λ_D in the scalar field results from a competition between the compression due to this strain field and diffusion of the scalar, giving $\lambda_D \sim (D/\varepsilon)^{1/2}$, with the result that $(\lambda_D/\lambda_\nu) \approx Sc^{-1/2}$, where $Sc \equiv (\nu/D)$. This picture of a strain-diffusion balance setting the finest lengthscales in the mixing of a scalar field is of course precisely the mechanism in Burgers (1948) and Townsend's (1951) solutions of sheets and lines as the canonical fine structure elements for the vorticity and kinetic energy dissipation fields in turbulent flows[†] . Indeed, in both these line and sheet solutions, the vorticity is merely a dynamically passive scalar quantity being advected by the flow and diffusing relative to the flow. As a consequence, these vortical line and sheet solutions are also candidates for the underlying canonical fine structure elements of passive scalar fields being mixed in turbulent flows.

[†] A discussion of these strain-limited solutions for vortex 'sheets' and 'lines' in steady strain fields is given by Sherman (1990); see his pp. 155-156 and pp. 564-567; see also Batchelor (1967) pp. 271-273. The extension to time-varying strain fields is given by Carrier, Fendell & Marble (1975); see their Eqs. (4.1) - (4.4).

Until recently, however, direct experimental measurements capable of discerning the scalar field fine structure in turbulent flows have not been possible. Dahm & Buch (1989, 1990) introduced fully resolved three-dimensional spatio-temporal measurements of Sc » 1 conserved scalar mixing, from which they concluded that the sheet-like solution referred to above forms the sole underlying canonical element of the scalar field fine structure. However, their experiments involved measurements in only two of the three spatial dimensions and thus, on the one hand, inherently underestimate the mixing rate when the scalar gradient has a strong component in the third spatial direction, and on the other hand required the assumption of isotropy in the scalar field to determine certain quantitative characteristics of the mixing. More recently, Dahm, Southerland & Buch (1990a,b,c) developed a technique for obtaining fully-resolved four-dimensional measurements of the space and time varying conserved scalar field in a turbulent flow, from which the true fine structure of the mixing process can be determined. This report summarizes measurements obtained with this technique and their use to analyze several aspects of the underlying fine structure of molecular mixing and chemical reactions in turbulent flows.

1.2 Formulation

In the mixing of any dynamically passive conserved scalar quantity ζ, the conserved scalar field $\zeta(\mathbf{x},t)$ satisfies the conservative advection-diffusion equation

$$\left[\frac{\partial}{\partial t}+\mathbf{u}\cdot\nabla-\frac{1}{ReSc}\nabla^2\right]\zeta(\mathbf{x},t)=0. \tag{1}$$

Here all variables have been made nondimensional by normalization with suitable reference outer flow length and velocity scales, l^* and u^*, and reference scalar value ζ^*. Note that (1) above involves only the product ReSc of the outer scale Reynolds number $Re \equiv (u^* l^*/\nu)$ and the Schmidt number $Sc \equiv (\nu/D)$, where ν and D are the vorticity and scalar diffusivities. However, the transport equation for $\mathbf{u}(\mathbf{x},t)$ introduces the Reynolds number explicitly as

$$\left[\frac{\partial}{\partial t}+\mathbf{u}\cdot\nabla-\frac{1}{Re}\nabla^2\right]\mathbf{u}(\mathbf{x},t)=-\frac{\nabla p}{\rho}\,, \tag{2}$$

and as a consequence the scalar field structure can in general depend on both Re and Sc. However, when normalization is done with the corresponding local inner scales of the flow, namely $l^* = \lambda_\nu$ and $u^* = (\nu/\lambda_\nu)$, then the inner scale Reynolds number is by definition unity. As a consequence, provided the scale separation between the local inner and outer flow scales is sufficiently wide (i.e. the local outer scale Reynolds number is sufficiently large), the velocity field $\mathbf{u}(\mathbf{x},t)$ on the inner scale should be independent of both the particular shear flow and of the outer Reynolds number. It is in this sense that the fine structure of the mixing and kinetic energy dissipation processes on the inner scales of

high Reynolds number turbulent flows are believed to be essentially universal (independent of the Reynolds number and of the particular flow). The inner scales of turbulent flows at Reynolds numbers sufficiently high for the scale separation to allow this universal structure to establish itself are generally beyond the reach of experimental resolution capabilities. Ultimately, the experimental resolution capability places a limit on the highest Reynolds number at which such fine structure measurements can be made. In the experimental investigation undertaken here, the objective is to obtain highly resolved measurements of the fine structure scales of the molecular mixing process in turbulent flows at flow conditions for which the Reynolds numbers are believed to be high enough that this universality begins to be approached.

From (1), the associated scalar energy per unit mass $^1/_2\zeta^2(\mathbf{x},t)$, defined analogous to the kinetic energy per unit mass $^1/_2u^2(\mathbf{x}.t)$, where $u \equiv |\mathbf{u}|$, follows the exact transport equation

$$\left[\frac{\partial}{\partial t}+\mathbf{u}\cdot\nabla-\frac{1}{ReSc}\nabla^2\right]\frac{1}{2}\zeta^2(\mathbf{x},t) = -\frac{1}{ReSc}\nabla\zeta\cdot\nabla\zeta(\mathbf{x},t)\ , \tag{3}$$

where the same conservative advection-diffusion operator appears on the left side, and where on the right side the term $(ReSc)^{-1}\nabla\zeta\cdot\nabla\zeta(\mathbf{x},t)$ gives the local instantaneous rate of scalar energy dissipation per unit mass, namely the rate at which non-uniformities in the scalar energy field are being reduced by molecular diffusion in the flow. In this context, the scalar dissipation is often adopted as a meaningful quantification for the local instantaneous rate of molecular mixing in the flow. Alternately, the scalar gradient magnitude $|\nabla\zeta(\mathbf{x},t)|$ is also sometimes used to define the mixing rate. Note that in terms of the scaled logarithm of the mixing rate, these two definitions become identical.

The concepts of scalar energy and its dissipation rate play a central role in many approaches for understanding and modeling molecular mixing and chemical reaction processes in turbulent flows. In particular, any reactive scalar in the flow [such as the mass fraction $Y_i(\mathbf{x},t)$ of any i-th species] will follow an advection-diffusion-reaction equation of the form

$$\left[\frac{\partial}{\partial t}+\mathbf{u}\cdot\nabla-\frac{1}{ReSc_i}\nabla^2\right]Y_i(\mathbf{x},t) = \dot{w}_i(\mathbf{x},t)\ , \tag{4}$$

where $w_i(\mathbf{x},t)$ is the local instantaneous reaction rate of species i. In many practical cases, the thermochemical state is determined entirely by the local instantaneous value of a conserved scalar ζ and a measure of the local time scale of the flow as

$$Y_i(\mathbf{x},t) = Y_i\big(\zeta(\mathbf{x},t);\ \nabla\zeta\cdot\nabla\zeta(\mathbf{x},t)\big)\,.$$

When this is the case, then from (1) and (4) the reaction rate of each species is given by

$$\dot{w}_i(\mathbf{x},t) = \left\{-\frac{1}{ReSc_i}\nabla\zeta\cdot\nabla\zeta(\mathbf{x},t)\right\}\left\{\frac{d^2Y_i}{d\zeta^2}\right\}_{\nabla\zeta\cdot\nabla\zeta}\,. \tag{5}$$

As a result, simultaneous knowledge of the precise structure of the conserved scalar field $\zeta(\mathbf{x},t)$ and the associated scalar dissipation field $\nabla\zeta\cdot\nabla\zeta(\mathbf{x},t)$ in a turbulent flow allow direct evaluation of the thermochemical structure and reaction progress in the flow.

Measurements of these quantities have in the past been difficult to obtain, principally due to two obstacles. First, determination of the true scalar gradient field $\nabla\zeta(\mathbf{x},t)$ and the associated scalar dissipation rate field $\nabla\zeta\cdot\nabla\zeta(\mathbf{x},t)$ requires measurement of the conserved scalar field $\zeta(\mathbf{x},t)$ in all three spatial dimensions. Second, since the dissipation rate is obtained by differentiation of the measured conserved scalar field, the spatial and temporal resolution of the original scalar measurements must be high enough to accurately resolve the finest length and time scales on which gradients in the scalar field are present in the flow. Beyond these requirements, the signal quality of the original scalar field measurements must also be high enough to permit accurate differentiation to determine the scalar gradient field.

1.3 Present Work

This study uses a laser imaging diagnostic, developed as part of this effort and specifically designed for very highly resolved, four-dimensional measurements, to obtain the full space- and time-varying conserved scalar field $\zeta(\mathbf{x},t)$ and the associated scalar energy dissipation rate field $\nabla\zeta\cdot\nabla\zeta(\mathbf{x},t)$ in a turbulent flow. This technique produces a four-dimensional (x-y-z-t) data space structured as shown in Figure 1. The resolution achieved between adjacent data points in each two-dimensional spatial data plane, and between adjacent data planes within each individual three-dimensional spatial data volume, as well as in time between the same plane in adjacent three-dimensional spatial data volumes in the four-dimensional data space, is finer than the local strain-limited molecular diffusion scale λ_D, allowing the fine structure of $Sc \gg 1$ molecular mixing in turbulent flows to be directly determined. The bulk of the measurements summarized here were obtained in the self-similar far field of an axisymmetric turbulent jet at an outer-scale Reynolds number $Re_\delta \equiv (u\delta/\nu)$ of 6000, as shown in Figure 2. Note, however, that the imaged region of the flow was quite small in comparison with the local outer scale δ, and was comparable to the inner scale λ_ν, of the flow. In particular, each data plane spanned approximately $^1/_{17}$ of the outer scale δ and approximately 1.6 times the inner scale λ_ν in both directions. As a result, if this outer-scale Reynolds number Re_δ is large enough so that on the inner scales $l^* \equiv \lambda_\nu$ and $u^* \equiv (\nu/\lambda_\nu)$, for which $Re \equiv 1$, the velocity $\mathbf{u}$ in Eqs. (1) - (3) has become independent of the outer-scale Reynolds number, then the scalar field fine structure would also be independent of Re_δ and would depend only on the Schmidt number. Furthermore, once the fine structure has become independent of the outer-scale Reynolds number, all memory of the outer scales is lost and the fine structure would then not be particular just to the turbulent jet, but should apply to mixing in turbulent shear flows in general. In this sense, we believe that many features of the fine

structure captured within our four-dimensional data space will to a large degree be generic to mixing in all high Reynolds number turbulent flows.

2.0 Experimental Technique

The experimental method developed for these measurements is an extension of our earlier work (Dahm & Buch 1989; Dahm & Buch 1990a, 1990b; Dahm, Southerland & Buch 1990) in obtaining highly resolved three-dimensional (256^3) spatio-temporal measurements of the conserved scalar concentration field and the resulting scalar energy dissipation rate field in turbulent flows. The technique is briefly described in the following section.

2.1 Diagnostic Method

The present experiments are of mixing in a turbulent shear flow in water. In particular, the bulk of the measurements conducted to date have been in the self-similar far field of an axisymmetric turbulent jet issuing into an essentially quiescent medium. The mixture fraction is defined here by the concentration of a dynamically passive dilute laser fluorescent dye (disodium fluorescein) carried by one of the fluids, and is a conserved scalar for which the Wilke-Chang method[††] suggests a value for the Schmidt number of 2075. In our experiments, this mixture fraction is measured repeatedly in time throughout a small three-dimensional volume in the flow by imaging the laser induced fluorescence from dye-containing fluid in the path of a laser beam rapidly swept in a raster fashion through the volume onto a high-speed planar photosensitive array. The measurements are conducted by issuing a jet through a round nozzle into a 0.8 m × 0.8 m × 1.8 m glass tank filled with water, in which a very small coflow (5.75 cm/min) insures that there is no recirculation of dyed fluid to contaminate the imaged volume in the flow. For this coflowing velocity, the measurement volume is approximately one coflow momenutm diameter downstream of the nozzle, placing it well within the pure jet limit of the flow (e.g. see Biringen 1975).

The successive laser induced fluorescence data planes can be rapidly acquired into gigabyte sized data sets using very fast computer disk ranks to produce a four-dimensional spatio-temporal data space structured as shown in Figure 1. Each such measured data space consists of a rapid succession of individual three-dimensional spatial data volumes. Each of these data volumes is itself composed of a sequence of two-dimensional spatial data planes, which in turn each consist of an array of 256 × 256 individual data points. The spatial separation between adjacent points within each data plane, and between adjacent data planes within each data volume, is smaller than the local strain-limited molecular

[††] See Mass Transfer, T.K. Sherwood, R.L. Pigford and C.R. Wilke, McGraw-Hill, New York, 1975.

diffusion lengthscale λ_D of the scalar field. Similarly, the temporal separation between adjacent data planes within each data volume, and between the same data plane in successive data volumes, is shorter than the local molecular diffusion scale advection time λ_D/u. This resolution, together with the high signal quality attained, allows accurate differentiation of the measured conserved scalar data in all three space dimensions and in time to determine the components of the local instantaneous scalar gradient vector field $\nabla\zeta(\mathbf{x},t)$ at every point in the data space. From this, the true instantaneous scalar energy dissipation rate field $\nabla\zeta\cdot\nabla\zeta(\mathbf{x},t)$ can be determined.

Key elements of the imaging and data acquisition system assembled for these four-dimensional measurements are shown schematically in Figure 3. A pair of very low inertia, galvanometric mirror scanners are used to synchronously sweep a collimated laser beam in a raster scan fashion through the desired volume in the flow field. The principal objectives of the scanner drive electronics are to synchronize the beam sweep with the photodiode array timing, so that each data plane corresponds to a single sweep of the beam, and to accommodate the minimum flyback times for the scanners within the period between acquisition of successive data planes. The horizontal and vertical sweep angles used are typically quite small; 0.125° and 4.26° respectively for our present measurements. The resulting laser induced fluorescence intensity is measured with a 256×256 imaging array, having center-to-center pixel spacings of $40\mu m$. The array is synchronized to the same clock that drives the scanners, and can be driven at variable pixel rates up to 11 MHz, allowing measurement of successive data planes at a continuous rate in excess of 140 planes per second. The fluorescence data from the array is serially acquired through a programmable digital port interface, digitized to 8-bits digital depth, then routed into a 16 MB high-speed dual-ported data buffer from which it can be continuously written in real time to a 3.1 GB high-speed parallel transfer disk rank. The overall sustained data throughput rate to the disks, accounting for all line and frame overhead cycles, is up to 9.3 MB/sec. The 3.1 GB disk capacity can accommodate more than 50,000 such measured 256×256 spatial data planes within the four-dimensional data space. Programmable gain and offset on the digital port interface allow the resulting data to span the full 8-bits of digital depth. The rms noise levels achieved are in all cases less than ± 1 digital signal level out of the 256.

2.2 Spatial and Temporal Resolution

Since the principal interest in these measurements is in obtaining the scalar dissipation field from the measured conserved scalar field via direct differentiation of the data, the central issue is the spatial and temporal resolution achieved by the measurements. From the measured thickness of the imaged portion of the laser beam, together with the pixel size and the image ratio of the measurements, the volume in the flow $(\Delta x\cdot\Delta y\cdot\Delta z)$ imaged onto each pixel can be determined. Furthermore, for the pixel clock rates used,

the time Δt between acquisition of successive data planes within each spatial data volume, and the time ΔT between the same data plane in successive data volumes, can also be determined. To assess the resulting relative resolution achieved, these smallest spatial and temporal scales discernible in the data must be compared with finest local spatial and temporal scales on which gradients in the conserved scalar field can be sustained in the flow. In particular, for local diffusion of vorticity in the presence of a time-varying strain rate $\varepsilon(t)$, the competing effects of strain and diffusion establish an equilibrium strain-limited vorticity diffusion layer thickness $\lambda_\nu \sim (\nu/\varepsilon)^{1/2}$, closely related to the Kolmogorov scale, giving the finest scale on which spatial gradients in the strain rate and vorticity fields can be locally sustained in the flow. A similar competition between the effects of strain and molecular diffusion of the conserved scalar establishes a local strain-limited molecular diffusion layer thickness $\lambda_D \sim (D/\varepsilon)^{1/2}$, related to the Batchelor scale and giving the smallest scale on which spatial gradients in the conserved scalar field can be sustained by the flow. The ratio of the vorticity and scalar diffusivities, ν and D respectively, establishes the relation between these two scales as $\lambda_D \sim \lambda_\nu \cdot Sc^{-1/2}$, where $Sc \equiv (\nu/D)$ is the Schmidt number and where, due to the similarity of the two strain-diffusion equilibrium processes, the proportionality constant should be approximately one. Note that, with the highest strain rates occurring locally in the flow scaling as $\varepsilon \sim (u/\delta) \cdot Re^{1/2}$, with $Re \equiv (u\delta/\nu)$ the local outer scale Reynolds number, the strain-limited diffusion scale in the conserved scalar field is $(\lambda_D/\delta) \sim Sc^{-1/2}\, Re^{-3/4}$. Measurements by Dowling (1988) give indications that the resulting proportionality constant is roughly 25.

The resolution requirements that Δx, Δy and Δz must be small compared to λ_D to allow meaningful differentiation in all three space directions within each three-dimensional spatial data volume, and that the time ΔT between the same data plane in successive data volumes must be small in comparison with the fine structure advection timescale (λ_D/u) to allow differentiation in time between data volumes, ultimately place a limit on the highest outer scale Reynolds numbers at which such fully resolved four-dimensional measurements are possible. Note that while the resolution Δx and Δy within each spatial data plane can in principle be made very small by simply reducing the image ratio, the resolution Δz is nominally determined by the laser beam thickness. There are clear limitations associated with the Rayleigh range of the optical resonator which determine how fine this can be made over the entire extent of the image volume. In general, the resulting minimum laser beam thickness is larger than the desired spatial separation between successive data planes. However, if the time Δt between successive planes is small enough so that the scalar field is effectively frozen, then the overlap in the measured scalar field between adjacent planes represents a convolution of the true scalar field with the laser beam profile. The measured scalar field can then be deconvolved with the measured beam profile shape to produce an effective resolution Δz comparable to the spatial separation between adjacent data planes, which is set by the horizontal scanner and can in principle be made quite small.

The present measurements were obtained at an axial location 235 jet momentum diameters (1.15 m) downstream of the jet source and a radial location 13 *cm* off the jet centerline. To estimate the resulting resolution requirements, we note that $\delta(x) \approx 0.44 \cdot x$ and $u(x) \approx 7.2\ (J/\rho)^{1/2} \cdot x^{-1}$, where J is the jet source momentum flux and ρ is the ambient fluid density. At the outer scale Reynolds number of 6000 and with the Schmidt number of 2075, these scalings give the local strain-limited molecular diffusion length-scale estimate of $\lambda_D \approx 407$ μm and the local advection timescale estimate of $(\lambda_D/u) \approx 100$ msec at the location of the measurement volume. With the measurements having an image ratio of 2.89, the in-plane spatial resolution was $\Delta x = \Delta y = 116$ μm. The $(1/e)$ laser beam thickness was measured as 380 μm, while the spatial resolution Δz between successive data planes was 220 μm. These Δx, Δy and Δz values must be compared with λ_D to assess the relative spatial resolution achieved. In particular note that, for the resulting pixel image volume, $(\Delta x \cdot \Delta y \cdot \Delta z)^{1/3}$ was nearly 3 times smaller than λ_D, while its maximum dimension (Δz) nearly 2 times smaller than λ_D. Similarly, the temporal separation between successive data planes was $\Delta t = 9.0$ msec and the time between successive data volumes was $\Delta T = 45$ msec, both of which are considerably smaller than the estimated local diffusion scale advection time of 100 msec. As a result, the present measurements should be capable of resolving essentially all of the fine scale structure of the local $Sc \gg 1$ turbulent mixing process.

3.0 Major Results

Analysis of four-dimensional data spaces of the type obtained here has many parallels with the analyses of large scale computational data volumes obtained from full numerical simulations of turbulent flows. Both can in principle be analyzed in considerable quantitative detail. However, a significant challenge facing both experiments and numerical simulations of this type is the extraction of insightful interpretations from such a very large amount of data. To this end we rely strongly on quantitative graphical visualization of large subsets of the original data space and numerically processed versions of it to provide guidance into the underlying physical process contained within the data. Here we choose to focus principally on the topology of the fine structure resulting from $Sc \gg 1$ scalar mixing in turbulent flows, and on the structural and associated statistical properties of the corresponding scalar gradient field.

3.1 Fine Scale Structure

Figure 4 shows the 8-bit conserved scalar data in three typical parallel adjacent 256 × 256 spatial data planes from the same data volume. The color levels denote the local conserved scalar value $\zeta(x,t)$ at each point, with pure blue corresponding to pure

ambient fluid ($\zeta = 0$) and increasing uniformly to pure red, corresponding to the highest scalar values in the data ($\zeta = 2.85\ \zeta_m$). Recall that each data plane shown spans approximately $^1/_{17}$ of the local outer scale $\delta(x)$, and approximately 1.6 times the local inner scale $\lambda_v(x)$, in each direction. The three spatial data planes are presented in order of increasing z (and therefore increasing time) in the clockwise direction, beginning at the upper left. Note that the relatively small change in the scalar field from one data plane to the next is a reflection of the relatively high temporal resolution of the measurements.

In Figure 5 we show the true scalar energy dissipation rate field $log\ \nabla\zeta\cdot\nabla\zeta(\mathbf{x},t)$ obtained by direct differentiation of the data in the three adjacent scalar planes in Figure 4. Linear central difference approximations have been used to evaluate the three components of the scalar gradient vector field $\nabla\zeta(\mathbf{x},t)$, with no explicit smoothing or filtering of the results. The dissipation field obtained is presented here in logarithmic form because this compression allows a wider range of mixing rates to be displayed. Additionally, we note that in logarithmic form the results are identical to those obtained if the mixing rate is alternately defined as $|\nabla\zeta(\mathbf{x},t)|$. The 256 different color levels now denote increasing values of the mixing rate. The first level, colored black, denotes zero and very low mixing rates, while the remaining levels range uniformly from blue through pure red denoting logarithmically increasing values of the local instantaneous scalar dissipation rate in the flow. For reference, pure red is scaled to the highest 0.1% of the dissipation rates and corresponds to $\nabla\zeta\cdot\nabla\zeta(\mathbf{x},t) = 5647.6\ (\zeta_m/\lambda_v)^2$. To examine the time evolution of the scalar energy dissipation rate field, in Figure 6 we show $log\nabla\zeta\cdot\nabla\zeta(\mathbf{x},t)$ in the same spatial data plane but from four temporally successive three-dimensional data volumes (see Figure 1). Time increases in the clockwise direction beginning at the upper left. Here the comparatively small change in the dissipation field between one data volume and the next, relative to the diffusion layer thickness, provides a clearer indication of the temporal resolution of the measurements.

The fine structure maps of the instantaneous scalar dissipation field in Figures 5 and 6 clearly show that essentially all of the molecular mixing occurs in thin sheet-like layers of the type described by Burgers and Townsend for the vorticity field. Both isolated and interacting layers can be seen. This appears to confirm the earlier conclusions of Dahm and Buch based on lower-dimensional measurements. Especially relevant in this connection are the broad features of relatively high dissipation near the center of the upper portion of the data planes in Figures 5 and 6. While these at first appear to not be layer-like structures, we find that most of the dissipation in these areas is due to the $(\partial\zeta/\partial z)^2$ contribution. In other words, the local scalar gradient vector is oriented largely normal to the data plane and corresponds to a layer-like structure which is cut nearly tangentially by the plane. All such layers oriented largely parallel to the data plane, as well as their contribution to the total mixing in the flow, are of course missed in lower-dimensional measurements of the dissipation. The internal structure of the molecular mixing within the layers apparent in Figures 5 and 6 can also be examined from our measurements, and this

confirms the earlier conclusions that strain-limited solutions of the Burgers and Townsend form give a remarkably accurate description of the true scalar energy dissipation profiles within these layers.

3.2 Isotropy

We next quantify the degree of anisotropy in the scalar gradient vector field captured in our four-dimensional data space by computing the probability densities for the square of each of the three components of $\nabla\zeta(\mathbf{x},t)$. The resulting distributions are shown in Figure 7. Note that y points in the upstream direction, x points radially outward. If the scalar field were fully isotropic, then all of these distributions would be identical, and it is clear that this is not the case. In particular, the average values of $(\partial\zeta/\partial x)^2$, $(\partial\zeta/\partial y)^2$ and $(\partial\zeta/\partial z)^2$ are respectively in the ratio (2.18) : (1.64) : (1.00), indicating that the gradient vector shows a tendency to point more toward the x-direction than either the y or z directions. This appears consistent with the fine structure of the scalar dissipation field in Figures 5 and 6, which show a preponderance of layers oriented somewhat more normal to the x-axis than toward the y or z axes. It appears likely that this does not represent an underlying anisotropy in the self-similar far field of turbulent jets, especially in view of the relatively small region of the flow spanned by each of the spatial data volumes (see Figure 2). Instead, this would seem more likely to be an indication of the somewhat marginal statistical significance of the relatively short time series represented by the temporal dimension of our four-dimensional data. We examine this in greater detail below.

We can view the anisotropy suggested by Figure 7 more directly in terms of the joint probability density $\beta(\vartheta,\varphi)$ of the spherical orientation angles ϑ and φ of the scalar gradient vector $\nabla\zeta(\mathbf{x},t)$, defined in Figure 8. The resulting joint distribution is shown in Figure 9, and the individual probability densities $\beta(\vartheta)$ and $\beta(\varphi)$ are shown in Figures 10a and 10b respectively. Note that, if the scalar field were fully isotropic and the gradient vector orientation were statistically independent of its magnitude, then the probability that the gradient vector in Figure 8 will point in any given direction would be the same for all directions, giving $\beta(\vartheta,\varphi) = {}^1/_{4\pi} \sin\varphi$, while $\beta(\vartheta) = {}^1/_{2\pi}$ and $\beta(\varphi) = {}^1/_2 \sin\varphi$. These general features are indeed identifiable in Figures 9 and 10. In particular, Figures 9 and 10a show an at least roughly sinusoidal variation in the distribution of φ obtained from the measurements. Note that the comparatively lower probability of φ being near 0 or π is consistent with the lower values of $(\partial\zeta/\partial z)$ noted above. Figures 9 and 10b show relatively little consistent variation in the observed distribution of ϑ save for the two peaks near 0 and π, corresponding to the same tendency noted in Figures 5–7 for the gradient vector to point more strongly in the x-direction.

Again, the anisotropy apparent in Figures 9 and 10 seems likely to be more a feature of the relatively short duration of the scalar field in our measurement than a feature of the overall scalar field itself. The relevant time scale for statistical significance within

such a small region of the flow appears likely to be on the order of a few strain-limited vorticity lengthscale advection times (λ_v/u). For the present data, the temporal dimension of the data space spans slightly less than $^1/_2$ (λ_v/u), so the fact that some anisotropy is seen here appears to be consistent with this comparison of timescales. Perhaps more important though is the observation that the results in Figures 7-10, and also those in Figure 11 below, approach the isotropy as closely as they do despite the comparison of timescales noted above, suggesting that the timescale required to achieve statistically isotropic scalar field data in a larger measurement of this type is indeed likely to be only a very few (λ_v/u).

3.3 Mixing Rate Distributions

The distributions in Figure 7 of the square of each component of the gradient vector are, in effect, one-dimensional estimates of the distribution of the true mixing rate $\nabla\zeta\cdot\nabla\zeta$. Such lower-dimensional measurements of the gradient vector $\nabla\zeta$ are typically used to approximate the scalar dissipation, since information in all three spatial dimensions is not generally available. In Figure 11, the mixing rate distributions that result from such one- and two-dimensional gradient approximations are compared with the result obtained from our fully three-dimensional measurement of the gradient. We note first that, for the lower-dimensional approximations, the discrete nature of the original 8-bit scalar measurements does not allow very low values of the dissipation to be accurately determined. This is especially true for the one-dimensional approximation, and thus these distributions have been truncated at the lowest discernible dissipation value. Irrespective of this effect, the one-dimensional approximation, and to a lesser degree the two-dimensional case, in principle have a long tail extending to the left and accounting for the spurious low dissipation values that would be obtained whenever the gradient vector has a comparatively large z-component (see Dahm & Buch 1989). If, however, the probability distribution $\beta(\vartheta,\varphi)$ of the scalar gradient vector orientations is known, then the one- and two-dimensional scalar dissipation distributions lead directly to the three-dimensional distribution. Furthermore, if the scalar field were truly isotropic, then the average values of the one-, two-, and three-dimensional dissipation distributions would be in the ratio (0.33) : (0.67) : (1.00). The actual average values obtained from Figure 11 are in the ratio (0.45) : (0.79) : (1.00), again indicating a degree of anisotropy in the comparatively short temporal extent of our measurement as noted above. Moreover, while the true scalar dissipation is generally assumed to be lognormally distributed, and thus its distribution would have a Gaussian shape in Figure 11, it is clear that the result obtained is not entirely lognormal. This too appears likely to be a manifestation of the marginal statistical significance of our four-dimensional data space.

3.4 Spottiness of the Dissipation Field

We can recognize in Figures 5 and 6 that the scalar energy dissipation field is not spatially homogeneous. This can be seen more clearly in Figure 12, where we show the dissipation field in linear form. Note that a very small fraction of the flow is occupied by high dissipation rates, corresponding to orange and red colorings. To directly quantify this 'spottiness' in the true scalar dissipation field, we show in Figure 13 the fraction of the total dissipation that occurs in any given volume fraction of the flow, obtained from the mixing rate distributions in Figure 11. Also shown are the results that would be obtained from the lower-dimensional measurements of the scalar dissipation in Figure 11. Notice that, in the lower-dimensional approximations of this result, manifestations of the anisotropy noted above can be seen. In particular, in a fully isotropic scalar field the one- and two-dimensional approximations should approach 0.33 and 0.67 respectively. Here the comparatively smaller z-component of the scalar gradient, apparent in Figures 5-10, renders the in-plane approximations somewhat higher than this. We also show in Figure 13 the curves for a lognormally distributed dissipation field, for which the result can be obtained analytically, as well as for a spatially homogeneous dissipation field, in which case the dissipation fraction is simply equal to the volume fraction.

Particularly noteworthy in Figure 13 is the result obtained from the true dissipation that just over 1% of the total volume of the flow accounts for nearly 10% of the total dissipation, while less than 12% of the total volume achieves 50% of the total dissipation, and 45% of the volume accomplishes nearly 90% of the dissipation. This rather strikingly quantifies the fact that a very small fraction of the flow accounts for the bulk of the mixing achieved. Viewed another way, 65% of the flow accomplishes less than 10% of the total mixing. Whether the result in Figure 13 will vary with increasing Reynolds number and from one flow to another, or whether instead the separation between the local outer scale δ and the inner scale λ_v in these measurements is large enough to achieve Reynolds number independence and flow independence on the scale of our data volume, remains an open question. The restrictions on the Reynolds number introduced by the resolution requirements preclude, at least for the present time, comparably resolved measurements at much higher Reynolds numbers.

3.5 Connection with Chaotic Advection

The picture emerging from our work of the universal small scale structure of mixing and reactions in turbulent shear flows as occurring in thin strained laminar diffusion layers bears a remarkable resemblance to certain features of the microstructure seen in recent experiments on mixing in low Reynolds number chaotic flows (e.g. Ottino, Leong, Rising & Swanson 1988; Ottino 1989; Ottino 1990). Those experiments find a "lamellar microstructure" that results from the stretching and folding of the scalar field due to the

due to the underlying chaotic dynamics of even comparatively simple periodic flows (including, among others, the classical "journal bearing flow" and the "cavity flow"). The dynamics in these flows that participate in the advection of scalar interfaces have been developed into a range of models for predicting various aspects of mixing and chemical reactions in these flows (e.g. Ottino et al 1988; Ottino 1989, Ottino 1990). The simultaneous observation of a highly folded layer-like fine structure in our present turbulent shear flows and in such low Reynolds number chaotic flows suggests a degree of universality in the fine scale structure of mixing that extends across the boundaries of the Reynolds number regimes traditionally associated with such comparatively simple chaotic flows and the turbulent flows investigated here.

To assess this possibility, we have conducted a preliminary comparison of the layer-like fine structure resulting from our four-dimensional measurements and the lamellar structures from Ottino's experiments on mixing in the cavity and journal bearing flows. In particular, in conjunction with J.M. Ottino, we have digitized several of scalar field slides of the cavity flow experiment and from these determined the associated scalar dissipation fields and examined the internal structure of the molecular diffusion layers. Sample results are shown in Figures 14 and 15. In particular, Figure 14 shows a relatively small region from the cavity flow, and in Figure 15 we have zoomed in on an even much smaller region of the flow. For comparison, Figure 15 also shows one of the dissipation field resulting from our present turbulent flow measurements.

It is essential to note at the outset that the resolution and signal quality in these very preliminary results are still far from what can be attained. No attempt had been made to adjust the imaging electronics to reduce the noise levels, and the illumination source used was far from uniform. Further experiments with more highly resolved slides are in progress, but several interesting conclusions can certainly be drawn even at this level of simplicity. First, over a region of the order of a few diffusion layer thicknesses in extent, dissipation fields in the chaotic flow show an overall structure that is very similar to that seen in turbulent flows. Furthermore, if we examine the internal structure of these diffusion layers we find that, to the level of resolution achieved in these preliminary comparisons, their internal structure appears to be essentially identical. Our present measurements give no direct information about the kinematical foundation for these layers, yet their presence is suggestive of a significant correlation between the scalar gradient vector direction and the most compressive principle strain rate axis which appears to form the basis of the lamellar microstructure in the chaotic flows.

3.6 Diffusion Layer Structure in Vortex Rings

A stable laminar vortex ring is formed when an impulse is imparted on a fluid in an axisymmetric manner, and has in the past been viewed as a particularly simple canonical structural element for the more complex vorticity field in fully turbulent flows. The

interest in vortex rings stems largely from the fact that the simple structure of the ring simultaneously lends itself well to experimental, theoretical, and numerical investigations. In this same sense, the vortex ring provides a relatively simple flow field, accessible to both experimental study and theoretical description, in which the understanding of the molecular mixing process in fluid flows can be also be examined and extended. Yet the mixing processes within such a laminar vortex ring do not appear to have been documented in any significant detail. There are of course several problems in which these mixing processes in the ring are of direct relevance, and many others for which they provide a simple canonical representation of potentially more complicated processes. In a broader sense, however, the laminar vortex ring provides a relatively simple and carefully controllable flow field in which the interaction of strain and diffusion on the mixing process can in principle be studied in considerable detail. For this reason, we have undertaken a study of the mixing of dynamically passive conserved scalar quantities in such an axisymmetric laminar vortex ring, giving a relatively detailed documentation based on experimental measurements of various features of the molecular mixing of such scalars in the ring, and focusing on their interpretation in terms of the dynamics of the associated mixing rate field.

Each ring was formed by discharging a volume of fluid through a round nozzle to form a thin cylindrical sheet of vorticity. This vortex sheet rolls up and develops into a stable ring that propagates away from the nozzle. The discharged fluid consisted of a uniform, weak, aqueous solution of a laser fluorescent dye (disodium fluorescein) that was pneumatically driven through a contoured axisymmetric nozzle by driving its free surface in a plenum with a high-pressure air stream metered through a micrometer-controlled, variable throat orifice held at sonic conditions with a constant upstream pressure. A solenoid valve in this high pressure air line was opened and closed via a variable delay timing circuit to discharge the dye-containing plenum fluid. For a given upstream pressure, the area of the sonic metering orifice set the air flowrate into the plenum, and the solenoid delay time (typically 50-100 ms) set the total amount of air supplied to the plenum. To keep the otherwise impulsive pressure rise driving the plenum fluid from exciting oscillations at the natural frequency of the second-order system formed by the compressibility of the air and the fluid mass in the plenum, the pressure rise was low-pass filtered by placing a volume of air in parallel with the plenum. This pneumatic drive arrangement allowed for a very low disturbance level and a high degree of symmetry in the vortex sheet generation and roll-up processes which form the ring. The nozzle had an exit diameter of 3.9 cm and produced rings with a center-to-center diameter $a \approx 4.9$ cm under all operating conditions. The ring circulation Γ was estimated from the integral of the exit velocity over time, and the corresponding Reynolds numbers $Re \equiv (\Gamma/\nu)$ were typically in the range from 5,000 to 10,000. The Schmidt number $Sc \equiv (\nu/D)$ for the dye solution in water is $O(10^3)$, giving $ReSc \approx O(10^7)$ in (1), (2) and (6). The details of the mixing process in the ring were measured with the same technique described in §2 of this

report.

The results from these measurements suggest that the evolution of the mixing process within such an axisymmetric laminar vortex ring can be usefully classified into three relatively distinct stages, namely *(i)* a ring generation stage, *(ii)* a 'pinch off' stage, and *(iii)* an asymptotic sta, e. We will summarize here only the major results obtained from the pinchoff and asymptotic stages; more complete details can be found in the full publication (Southerland, Porter, Dahm & Buch 1991). The 'pinch off 'stage is characterized by the diffusional cancellation between adjacent strained molecular diffusion layers, which occurs in turbulent flows also. In particular, from (1) the scalar dissipation field in (2) can be seen to follow the exact transport equation

$$\left[\frac{\partial}{\partial t}+\mathbf{u}\cdot\nabla-\frac{1}{ReSc}\nabla^2\right]\frac{1}{2}(\nabla\zeta\cdot\nabla\zeta) = -(\nabla\zeta\cdot\boldsymbol{\varepsilon}\cdot\nabla\zeta)-\frac{1}{ReSc}\nabla(\nabla\zeta):\nabla(\nabla\zeta) \qquad (6)$$

where the same conservative advection-diffusion operator is on the left. In the first term on the right, $\boldsymbol{\varepsilon} \equiv {}^1/_2(\nabla\mathbf{u} + \nabla\mathbf{u}^T)$ is the local strain rate field, and the contraction simply selects the normal strain rate along the scalar gradient vector direction as $-\varepsilon_{\nabla\zeta\nabla\zeta}(\nabla\zeta\cdot\nabla\zeta)$. The remaining components of the strain rate act only to change the gradient vector orientation, but do not affect its magnitude. In this form, it can be readily seen that this term simply accounts for the reduction in scalar gradient magnitude due to extensional straining along the gradient direction, or conversely the increase in dissipation that results when the scalar gradient is compressed. The second term on the right in (6) is strictly negative, and gives the reduction in dissipation due to diffusional cancellation of gradients in the scalar dissipation field. It is this term that plays a key role in determining the evolution of the mixing rate field at various stages in the ring.

Data detailing the dynamics of this diffusional cancellation process are shown in Figure 16, where for brevity we present results for the mixing rate field *log* $\nabla\zeta\cdot\nabla\zeta(\mathbf{x},t)$ only. The sequence shown consists of every 20th frame from the imaging measurements, corresponding to a time interval between successive panels of $(\Delta t\cdot\Gamma/2\pi a^2) \approx 0.089$, and beginning at roughly the end of the ring formation stage. The quantitative color values are assigned as shown, with the highest 0.1% of the mixing rates again corresponding to pure red. The key feature in this phase is the cancellation between the two scalar dissipation layers seen in this diametral plane which intersects the initially cylindrical dissipation surface emanating from the nozzle. In the sequence in Figure 16, this cancellation is most readily apparent between the two dissipation layers which at this time still connect the ring to the nozzle. At relatively early times these layers are still widely separated, but the strain field induced by the ring then begins to draw them together on a relatively fast time scale. A short time later, the two layers begin to interact strongly and, owing to the cancellation term in (6), the mixing rate rapidly drops to zero. Beyond this point, the ring is no longer 'connected' to the nozzle and all of the plenum fluid that will eventually reside in the Kelvin oval has been committed to the ring. The ambient fluid

trapped between the streamlines passing through the forward and rearward stagnation points then simply continues to wrap on an increasingly finer scale with this plenum fluid during the asymptotic stage.

Overall, the dynamics of the scalar dissipation layers in Figure 16 bear a strong resemblance to the anticipated dynamics of the vorticity field associated with the ring pinchoff process. Indeed, there is a similarity in the dynamics of the vorticity and scalar dissipation fields. In particular, note that (6) for the scalar dissipation $\nabla\zeta\cdot\nabla\zeta$ is very similar to the transport equation for the square of the vorticity magnitude $\boldsymbol{\omega}\cdot\boldsymbol{\omega}$, sometimes referred to as the enstrophy, which takes the form

$$\left[\frac{\partial}{\partial t}+\mathbf{u}\cdot\nabla-\frac{1}{Re}\nabla^2\right]\frac{1}{2}(\omega\cdot\omega) = (\omega\cdot\varepsilon\cdot\omega)-\frac{1}{Re}\nabla\omega:\nabla\omega \qquad (7)$$

Comparison with (6) shows that the symmetric contraction in the first term on the right now selects the normal strain rate along the vorticity vector direction, namely $+\varepsilon_{\omega\omega}(\boldsymbol{\omega}\cdot\boldsymbol{\omega})$. The further difference in sign reflects the fact that extensional strain along the vorticity vector direction acts to increase its magnitude. Here, due to the axisymmetry of the ring, the scalar gradient and vorticity vectors will lie normal to each other, and thus the component of the strain rate that affects their evolution will be different. Interestingly though, in flows where $\nabla\zeta$ and $\boldsymbol{\omega}$ are aligned, the dynamics of the scalar dissipation at a given value of the dimensionless scalar diffusivity $ReSc$ will be entirely parallel those of the vorticity magnitude when Re is increased to this same value. Of course, in the vortex ring, the initial condition for the scalar dissipation includes a nonzero disk in the nozzle exit plane that has no parallel in the vorticity field.

Aside from the diffusional cancellation noted above, there is of course additional cancellation of this type that begins where the dissipation layer extending from the forward stagnation point meets the remnants of the layers that originally were connected to the nozzle lip. This cancellation of the mixing rate within these layers continues along the spiral arms as these two layers wrap around each other in their approach toward the vortex core. As a consequence, the mixing rate begins to drop rapidly as the center of the core is approached. This will be seen more clearly in the discussion of the asymptotic stage given below. One last point regarding the pinch off stage is important here. Notice that the two layers emanating from the nozzle do not remain symmetrically located around the centerline of the ring. Except at the earliest times in this stage, the layers consistently wander off the centerline, especially near the forward stagnation point. This appears to be due to the fact that this is a hyperbolic point, and as a result the flow along streamlines approaching it is sensitive to even very small displacements from the centerline. The effect of any slight initial asymmetry that causes these two layers not to pinch off precisely on this dividing streamline will therefore show a large displacement when integrated over time, even though the underlying flow field is very nearly symmetric.

Once the ring has pinched off, the ambient fluid trapped inside the Kelvin oval

wraps up with the plenum fluid on an increasingly finer scale along the two spiral arms extending toward the center of the core. This can be seen quite clearly in Figures 17a and 17b, which respectively show the scalar and scalar dissipation fields in the right half of the ring during the 'asymptotic stage' where the ring has already wrapped up to a rather large degree. As the axes indicate, the image covers only the right half of the ring, with the centerline coinciding roughly with the left edge of the image and the vertical axis referenced to the core location z_c. The number of windings seen now give an indication of the dimensionless 'age' of the ring. Note that the color values are assigned as shown, with ζ^* denoting the average scalar value of the fluid inside the Kelvin oval, determined without radial weighting in the plane. The primary dynamical feature during this stage of the ring evolution is the continual lengthening of the two spiral arms leading to the core in Figure 17a. This extensional straining of the scalar dissipation layers in Figure 17b between these arms leads to a compressional straining along the layer normal direction. This in turn creates a steepening of the gradient scale and a corresponding increase in the gradient magnitude. Eventually the thickening effect of diffusion acts to balance the thinning due to the strain, and the result is a strain-limited molecular diffusion layer thickness. In Figure 17b this balance between diffusion and the strain field imposed by continuity appears to establish a thickening of the layers as they rotate through the upper half of the ring from the furthest outboard point back toward the centerline, and then a thinning of the layers as they rotate back through the lower half of the ring. The scalar dissipation values furthest from the centerline of the ring also appear to be consistently lower than those closest to the centerline, presumably due to diffusional cancellation between the layers. This also leads to a rapid drop in the scalar dissipation within the layers as the center of the core is approached. Indeed, the scalar values in both arms of the spiral can be seen to approach the green value attained at the center of the core. Note in particular that even the core center appears to be adequately resolved, suggesting that the scalar dissipation field is sufficiently resolved throughout the ring to allow accurate determination of the fine structure of the mixing process. There is, moreover, a pattern of alternating high and low dissipation rates encountered as the core is approached along the layer normal direction. However, it is not clear if this results from the different strain rate histories to which the two scalar dissipation layers that originally emanated from the forward stagnation point and from the nozzle were subjected, or if instead this is a remnant of the initial conditions.

3.6 Scalar Imaging Velocimetry (SIV)

Equation (1) shows the effect of the underlying velocity field on the mixing process within the ring. It is possible to use these relatively high resolution scalar field measurements to invert (1) and extract a limited type of information about the velocity field underlying the mixing process. In particular, since the velocity affects the scalar field

only through the $\mathbf{u}\cdot\nabla\zeta$ term in(1), the scalar field is affected only by the velocity component $u_{||}(\mathbf{x},t)$ oriented along the local gradient vector orientation. Inverting the conserved scalar transport equation gives this velocity component in terms of the measured scalar field $\zeta(\mathbf{x},t)$ as

$$u_{||}(\mathbf{x},t) = \left[\frac{1}{ReSc}\nabla^2\zeta - \frac{\partial\zeta}{\partial t}\right] \Big/ |\nabla\zeta| \tag{8}$$

Note that this involves not only the scalar gradient field examined thus far, but also the Laplacian and the time derivative of the scalar field. If measurements such as these have a spatial resolution that is sufficiently high to allow accurate determination of the second derivatives in the Laplacian, and at the same time have a sufficiently fine temporal separation between successive images in time to allow meaningful evaluation of the time derivative of the scalar field, then in principle (8) will allow the velocity component $u_{||}(\mathbf{x},t)$ to be determined. Notice, however, that this inversion is only possible where the scalar gradient is not zero. We point out also that the velocity $u_{||}(\mathbf{x},t)$ in (8) is physically different from the notion of an isoscalar surface velocity discussed by Gibson (1968), for which the time derivative does not appear.

In Figure 18 we show each of the component fields involved in the inversion in (8). The color values in each case denote linearly increasing values of the absolute magnitude of the component field, and no explicit smoothing or filtering has been applied to any of these fields. Figure 18a shows the original scalar field $\zeta(\mathbf{x},t)$ during a relatively early stage in the pinch off phase. The resulting scalar gradient magnitude $|\nabla\zeta(\mathbf{x},t)|$ is shown in Figure 18b. Numerically evaluating the divergence of this scalar gradient field, again using linear central difference approximations, yields the Laplacian field $\nabla^2\zeta(\mathbf{x},t)$ shown in Figure 18c. Here it can be seen that the original scalar field data are sufficiently highly resolved to allow a relatively smooth determination even of these second derivatives. We note, however, that the relatively high value of $ReSc$ involved in these measurements renders the contribution of the Laplacian in (8) practically negligible, and thus the requirement that second derivatives of the measured data need to be accurately obtainable can in practice be relaxed. As far as the time derivative $\partial\zeta/\partial t$ is concerned, we also approximate this with a linear central difference among the scalar field image immediately before and immediately after that shown in Figure 18a, with the result shown in Figure 18d.

From the component fields in Figure 18, the inversion in (8) can be evaluated to determine $u_{||}(\mathbf{x},t)$. The result is shown in Figure 19, where the colors denote linearly increasing values of $u_{||}$, and where points at which the scalar gradient magnitude in Figure 18b is essentially zero have been flagged red to show where the inversion is not possible. Note also that the $u_{||}(\mathbf{x},t)$ is presented in the original lab-fixed frame. The result obtained shows relatively high values along the upstream and downstream sectors of the ring, where the scalar gradient lies coincident with the direction of propagation, and much

smaller values where the gradient vector is oriented largely normal to the propagation direction. In principle, of course, continuity can be used to extract information about the remaining velocity component $u_{\perp}(\mathbf{x},t)$ from the result obtained for $u_{\parallel}(\mathbf{x},t)$ in Figure 19, since the velocity at the center of the core is known from the propagation speed of the ring. We note that this would allow the strain rate tensor field $\boldsymbol{\varepsilon}(\mathbf{x},t)$ to be evaluated within the ring, and thereby permit a far more detailed quantitative study of the interaction between the strain field and the molecular mixing in the ring than the documentation of the mixing processes undertaken thus far.

4.0 Publications

The following publications have resulted in part from the research efforts described in this report. These also describe additional work and give further technical details beyond what is possible in the brief overview given in this report.

1. Southerland, K.B., Porter, J.R., Dahm, W.J.A. & Buch, K.A. (1991) "An experimental study of the molecular mixing process in an axisymmetric laminar vortex ring," to appear in *Physics of Fluids A*.

2. Tryggvason, G. and Dahm, W.J.A. (1991) "An integral method for mixing, chemical reactions, and extinction in unsteady strained diffusion layers," to appear in *Combustion and Flame*.

3. Tryggvason, G. and Dahm, W.J.A., "Fine structure of vortex sheet rollup by viscous and inviscid simulation," to appear in *ASME Journal of Fluids Engineering*.

4. Dahm, W.J.A., Southerland, K.B. & Buch, K.A. (1991) "Four-dimensional laser induced fluorescence measurements of conserved scalar mixing in turbulent flows," to appear in *Applications of Laser Techniques to Fluid Mechanics*, R. Adrian, Ed. Springer Verlag, Berlin.

5. Dahm, W.J.A., Southerland, K.B. & Buch, K.A. (1990) "Direct, high-resolution, four-dimensional measurements of the fine scale structure of Sc » 1 molecular mixing in turbulent flows," submitted to *Physics of Fluids A*.

6. Chang, C.H.H., Dahm, W.J.A. and Tryggvason, G. (1990) "Lagrangian model simulations of molecular mixing, including finite rate chemical reactions, in a temporally developing shear layer," submitted to *Physics of Fluids A*.

7. Dahm, W.J.A. & Buch, K.A. (1991) "Fine scale structure of conserved scalar mixing in turbulent shear flows. Part I: Sc » 1." To be submitted to *Journal of Fluid Mechanics*.

8. Dahm, W.J.A. & Buch, K.A. (1991) "Fine scale structure of conserved scalar mixing in turbulent shear flows. Part II: Sc ≈ 1." To be submitted to *Journal of Fluid Mechanics*.

9. Dahm, W.J.A., Southerland, K.B. & Buch, K.A. (1990) "Four-dimensuional laser induced fluorescence measurements of conserved scalar mixing in turbulent flows," *Proceedings of the 5th International Symposium on Applications of Laser Techniques in Fluid Mechanics*, pp. 1.1.1-1.1.6, Instituto Superior Técnico, Lisbon, Portugal.

10. Southerland, K.B., Porter, J.R., Dahm, W.J.A. & Buch, K.A. (1990) "An experimental study of the molecular mixing process in an axisymmetric laminar vortex ring," *Proceedings of the IUTAM Symposium on Fluid Mechanics of Stirring and Mixing*, Paper No. PD-9, University of California (San Diego), La Jolla, CA.

11. Dahm, W.J.A., Southerland, K.B. & Buch, K.A. (1990) "Direct, high-resolution, four-dimensional measurements of the fine scale structure of Sc » 1 molecular mixing in turbulent flows," *Proceedings of the IUTAM Symposium on Fluid Mechanics of Stirring and Mixing*, Paper No. PB-4, University of California (San Diego), La Jolla, CA.

12. Chang, C.H.H., Dahm, W.J.A. and Tryggvason, G. (1990) "Lagrangian model simulations of molecular mixing, including finite rate chemical reactions, in a temporally developing shear layer," *Proceedings of the IUTAM Symposium on Fluid Mechanics of Stirring and Mixing*, Paper No. PC-8, University of California (San Diego).

13. Dahm, W.J.A., Buch, K.A., Dibble, R.W., Fourguette, D.C. and Barlow, R.S., (1990) "Fully resolved instantaneous laser Rayleigh imaging measurements of conserved scalar mixing in lifted turbulent diffusion flames," *Twenty-third International Symposium on Combustion*, Poster Paper No. P212, The Combustion Institute, Pittsburgh, PA.

14. Chang, C.H.H., Dahm, W.J.A. and Tryggvason, G. (1990) "A Lagrangian model for simulating combustion, including finite rate chemistry, in complex flows," *Twenty-third International Symposium on Combustion*, Poster No. Paper P229, The Combustion Institute, Pittsburgh, PA, (1990).

15. Dahm, W.J.A., Buch, K.A., Dibble, R.W., Fourguette, D.C. & Barlow, R.S. (1989) "Structure of the Scalar Dissipation Field for Mixing of a Sc ≈ 1 Conserved Scalar in a Turbulent Shear Flow," *Bull. Am. Phys. Soc.* 34, 2264.

16. Buch. K.A. & Dahm, W.J.A. (1989) "Scalar Dissipation Field in a Trubulent Shear Flow with Sc » 1," *Bull. Am. Phys. Soc.* 34, 2264.

17. Chang, C.H.H., Dahm, W.J.A. and Tryggvason, G. (1990) "Lagrangian Model Simulation of Molecular Mixing, Finite Rate Chemical Reactions and Extinction, in a Temporally Developing Shear Layer," *Bull. Am. Phys. Soc.* 35, 2319.

18. Southerland, K.B. & Dahm, W.J.A. (1990) "Four-Dimensional Measurements of the Conserved Scalar Field in a Turbulent Flow," *Bull. Am. Phys. Soc.* 35, 2287.

19. Sbeih, K., Tryggvason, G. & Dahm, W.J.A. (1990) "Numerical Simulations of Viscous and Inviscid Kelvin-Helmholtz Instability," *Bull. Am. Phys. Soc.* 35, 2253.

20. Buch, K.A. & Dahm, W.J.A. (1990) "Turbulent Diffusion Flame Structure from Conserved Scalar Measurements," *Bull. Am. Phys. Soc.* 35, 2319.

21. Dahm, W.J.A. & Buch, K.A. (1989) "Structure of the Scalar Dissipation Field for Mixing of Sc ≈ 1 and Sc » 1 Conserved Scalar Fields in Turbulent Shear Flows: Stretching and Folding of Molecular Diffusion Layers," Poster Presentation, *Forty-second Annual Meeting, Division of Fluid Dynamics, American Physical Society*, Palo Alto, CA.

References

Batchelor, G.K. (1967) *In Introduction to Fluid Dynamics*. Cambridge Univ. Press, Cambridge.

Batchelor, G.K. (1959) Small-scale variation of convected quantities like temperature in a turbulent fluid. Part 1. General discussion and the case of small conductivity. *J. Fluid Mech.* 5, 113-133.

Biringen, S. (1975) An experimental study of a turbulent axisymmetric jet issuing into a coflowing airstream. *VKI Technical Note 110.*

Burgers, J.M. (1948) A mathematical model illustrating the theory of turbulence. *Adv. Appl. Mech.* 1, 171-199.

Carrier, G.F., Fendell, F.E., & Marble, F.E. (1975) The effect of strain rate on diffusion flames. *SIAM J Appl. Math.* 28, 463-500.

Dahm, W.J.A. & Buch, K.A. (1989) High resolution three-dimensional (256^3) spatio-temporal measurements of the conserved scalar field in turbulent shear flows. *Proc. 7th Symp. on Turbulent Shear Flows* 1, 14.1.1-14.1.6.

Dahm, W.J.A. & Buch, K.A. (1990) High resolution three-dimensional (256^3) spatio-temporal measurements of the conserved scalar field in turbulent shear flows. To appear in *Turbulent Shear Flows 7*, Springer, Berlin.

Dahm, W.J.A. and Buch, K.A. (1989) Lognormality of the scalar dissipation pdf in turbulent flows. Phys. Fluids A, Vol. 1, No. 7, pp. 1290 – 1293.

Dahm, W.J.A., Southerland, K.B. and Buch, K.A. (1991) Direct, high resolution, four-dimensional measurements of the fine scale structure of Sc » 1 molecular mixing in turbulent flows. Submitted to Phys. Fluids A.

Dahm, W.J.A., Southerland, K.B. and Buch, K.A. (1990) Direct, high resolution, four-dimensional measurements of the fine scale structure of Sc » 1 molecular mixing in turbulent flows. *Proceedings of the IUTAM Symposium on Fluid Mechanics of Stirring and Mixing*, Invited Paper No. PB-4, UC San Diego, La Jolla, CA.

Dahm, W.J.A., Southerland, K.B. and Buch, K.A. (1990) Four-dimensional laser induced fluorescence measurements of conserved scalar mixing in turbulent flows.

Proceedings of the 5th International Symposium on Applications of Laser Techniques to Fluid Mechanics, pp. 1.1.1 – 1.1.6, Instituto Superior Técnico, Lisbon, Portugal.

Dahm, W.J.A., Southerland, K.B. and Buch, K.A. (1991) Four-dimensional laser induced fluorescence measurements of conserved scalar mixing in turbulent flows. To appear in *Applications of Laser Techniques to Fluid Mechanics*, R. Adrian, Ed., Springer, Berlin.

Dahm, W.J.A. & Buch, K.A. (1991) Fine scale structure of conserved scalar mixing in turbulent flows. Part I: Sc » 1. In preparation for *J. Fluid Mech*

Dahm, W.J.A. & Buch, K.A. (1991) Fine scale structure of conserved scalar mixing in turbulent flows. Part II: Sc ≈ 1. In preparation for *J. Fluid Mech.*

Dowling, D.R. (1988) Mixing in gas phase turbulent jets. *Ph.D. Thesis*, Caltech, Pasadena, CA.

Gibson, C.H. (1968a) Fine structure of scalar fields mixed by turbulence. I. Zero-gradient points and minimal-gradient surfaces. *Phys. Fluids* 11, 2305-2315.

Kolmogorov, A.N. (1941) Local structure of turbulence in an incompressible fluid at very high Reynolds numbers. *C.R. Acad. Sci. URSS* 30, 301-305.

Ottino, J.M. (1989) *The kinematics of mixing: stretching, chaos, and transport.* Cambridge Univ. Press.

Ottino, J.M. (1982) Description of mixing with diffusion and reaction in terms of the concept of material surfaces. *J Fluid Mech.* 114, 83-103.

Ottino, J.M. (1989) The mixing of fluids. *Scientific American* January 1989, 56-67.

Ottino, J.M. (1990) Mixing, chaotic advection, and turbulence. *Ann. Rev. Fluid Mech.* 22, 207-253.

Ottino, J.M., Leong, C.W., Rising, H. & Swanson, P.D. (1988) Morphological structures produced by mixing in chaotic flows. *Nature* 333, 419-425.

Sherman, F.S. (1990) *Viscous Flow.* McGraw-Hill, New York.

Southerland, K.B., Porter, J.R., Dahm, W.J.A. and Buch, K.A. (1991) An experimental study of the molecular mixing process in an axisymmetric laminar vortex ring. To appear in Phys. Fluids A.

Southerland, K.B., Porter, J.R., Dahm, W.J.A. and Buch, K.A. (1990) An experimental study of the molecular mixing process in an axisymmetric laminar vortex ring. *Proceedings of the IUTAM Symposium on Fluid Mechanics of Stirring and Mixing*, Poster Paper No. PD-9, UC San Diego, La Jolla, CA.

Townsend, A.A. (1951) On the fine-scale structure of turbulence. *Proc. Roy. Soc. Lond. A* 208, 534-542.

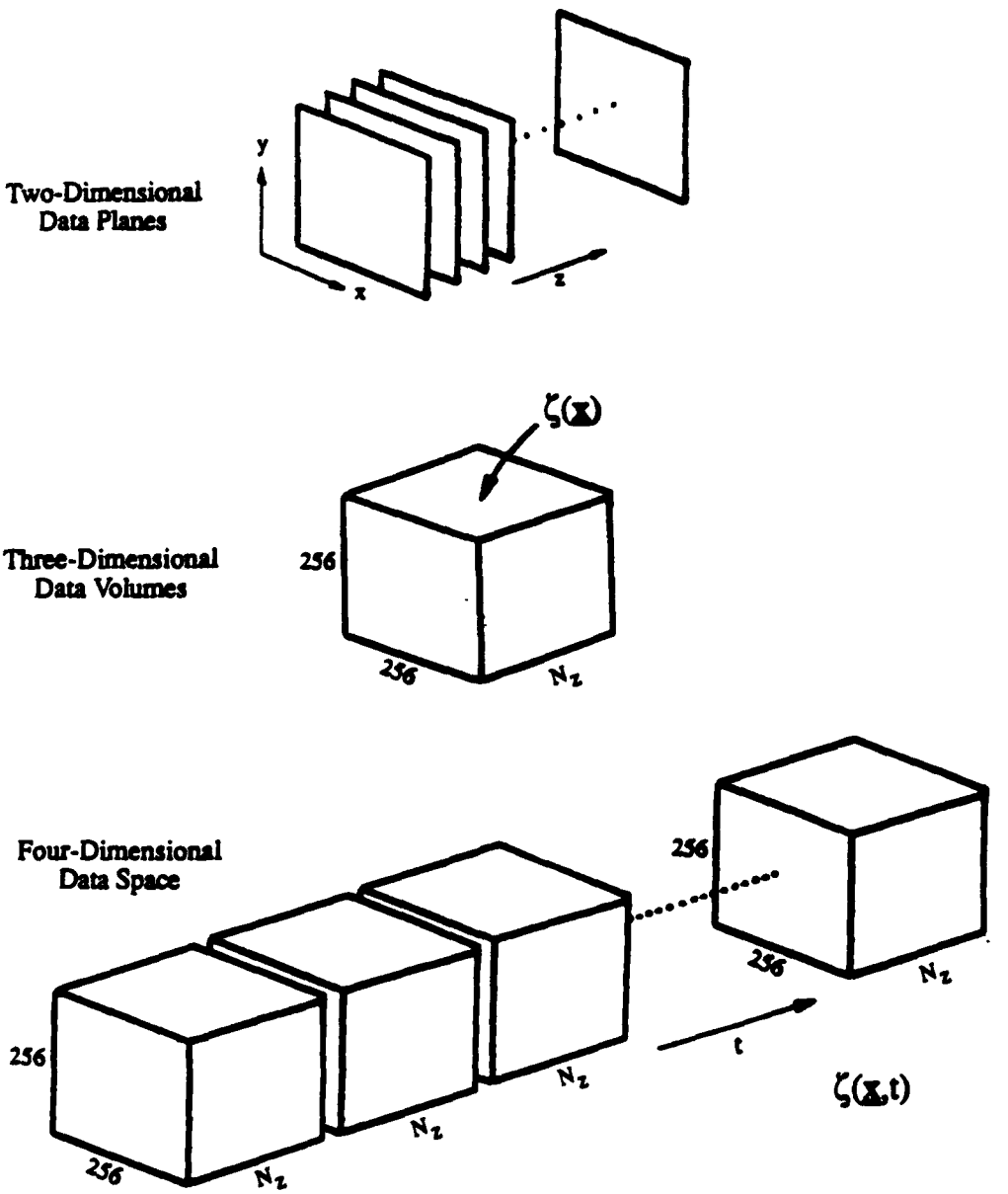

Fig. 1 . Structure of the experimentally measured, four-dimensional, spatio-temporal conserved scalar data space $\zeta(x,t)$ as a temporal progression of three-dimensional spatial data volumes, each consisting of a sequence of two-dimensional spatial data planes, each composed of a 256×256 array of data points. The spatial and temporal resolution achieved is sufficient to allow direct differentiation of the conserved scalar data in all three space dimensions and in time, allowing the evolution of the true molecular mixing rate field $\nabla\zeta \cdot \nabla\zeta(x,t)$ to be directly determined.

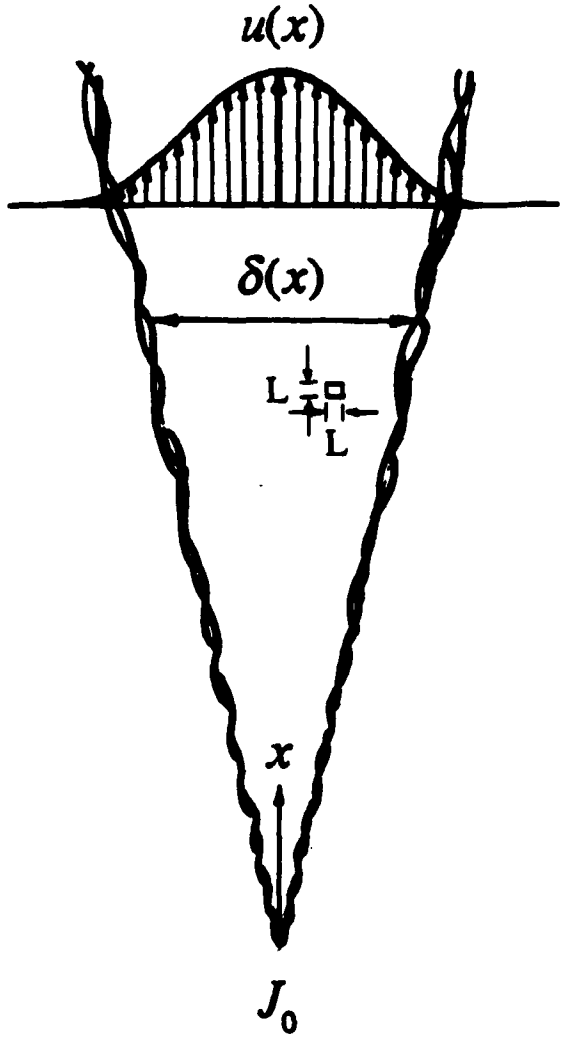

Fig. 2. The scalar field is measured in the self-similar far field of an axisymmetric turbulent jet in water at an outer-scale Reynolds number Re_δ of 6,000. The approximate size (L) and location of the imaged region of the flow are indicated. In terms of the local outer scale of the flow, $(L/\delta) \approx 1/17$, while in terms of the local inner scale, $(L/\lambda_v) \approx 1.6$. As a result, if Re_δ is large enough so that all memory of the outer scales u and δ is lost on the inner scale of the flow, then the fine structure results obtained from the imaged region will to a large degree be generic to $Sc \gg 1$ mixing in all high Reynolds number turbulent flows.

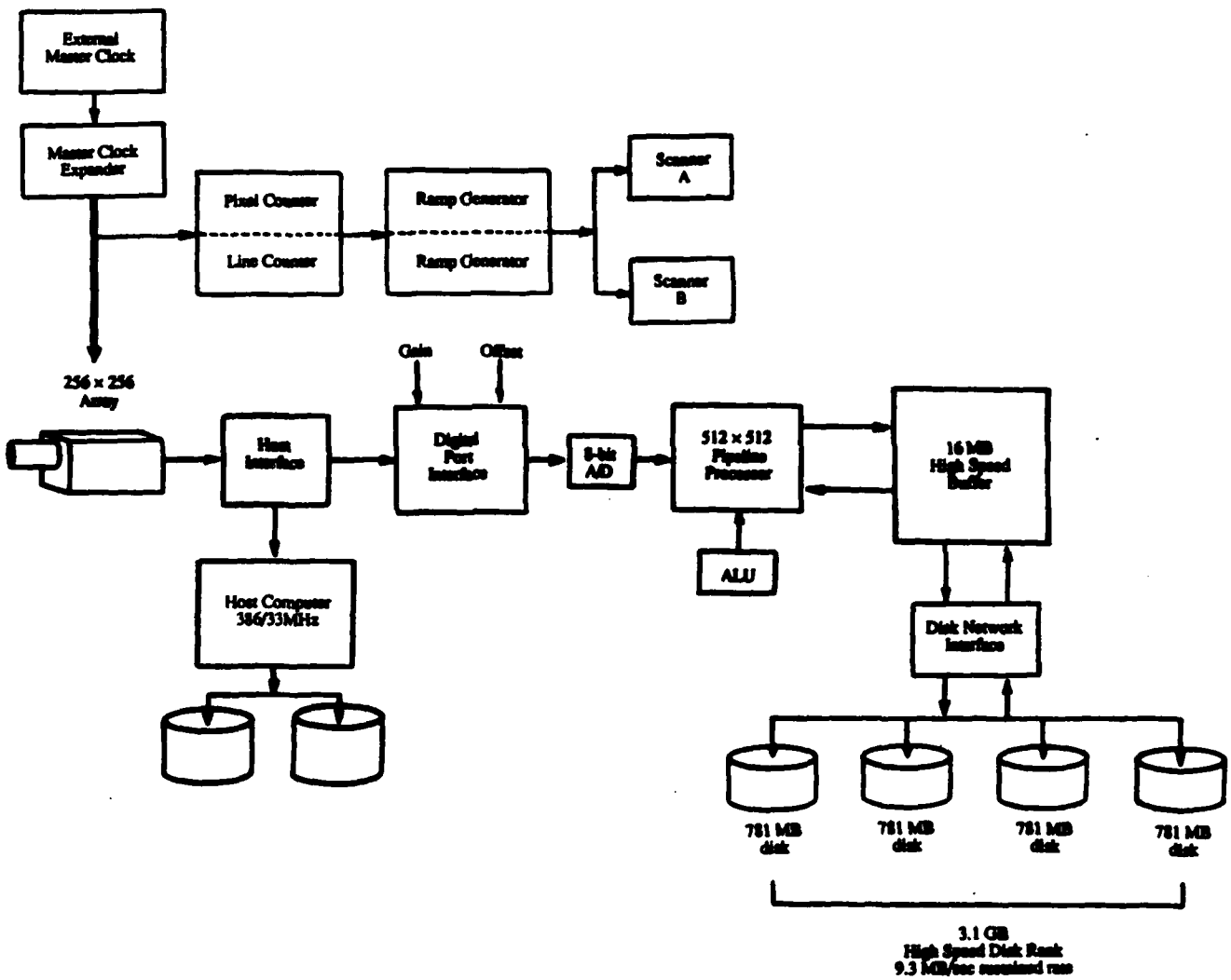

Fig. 3. Key elements of the high-speed variable-rate imaging and data acquisition system assembled for these fully-resolved four-dimensonal measurements of scalar mixing in turbulent flows. Two low-inertia galvanometric mirror scanners are slaved to the imaging array timing to rapidly sweep the laser beam in a successive raster scan fashion through the scalar field. The data acquisition system can achieve a sustained data throughput rate to the disk bank of up to 9.3 MB/sec for volumes as large as the full 3.1 GB disk capacity.

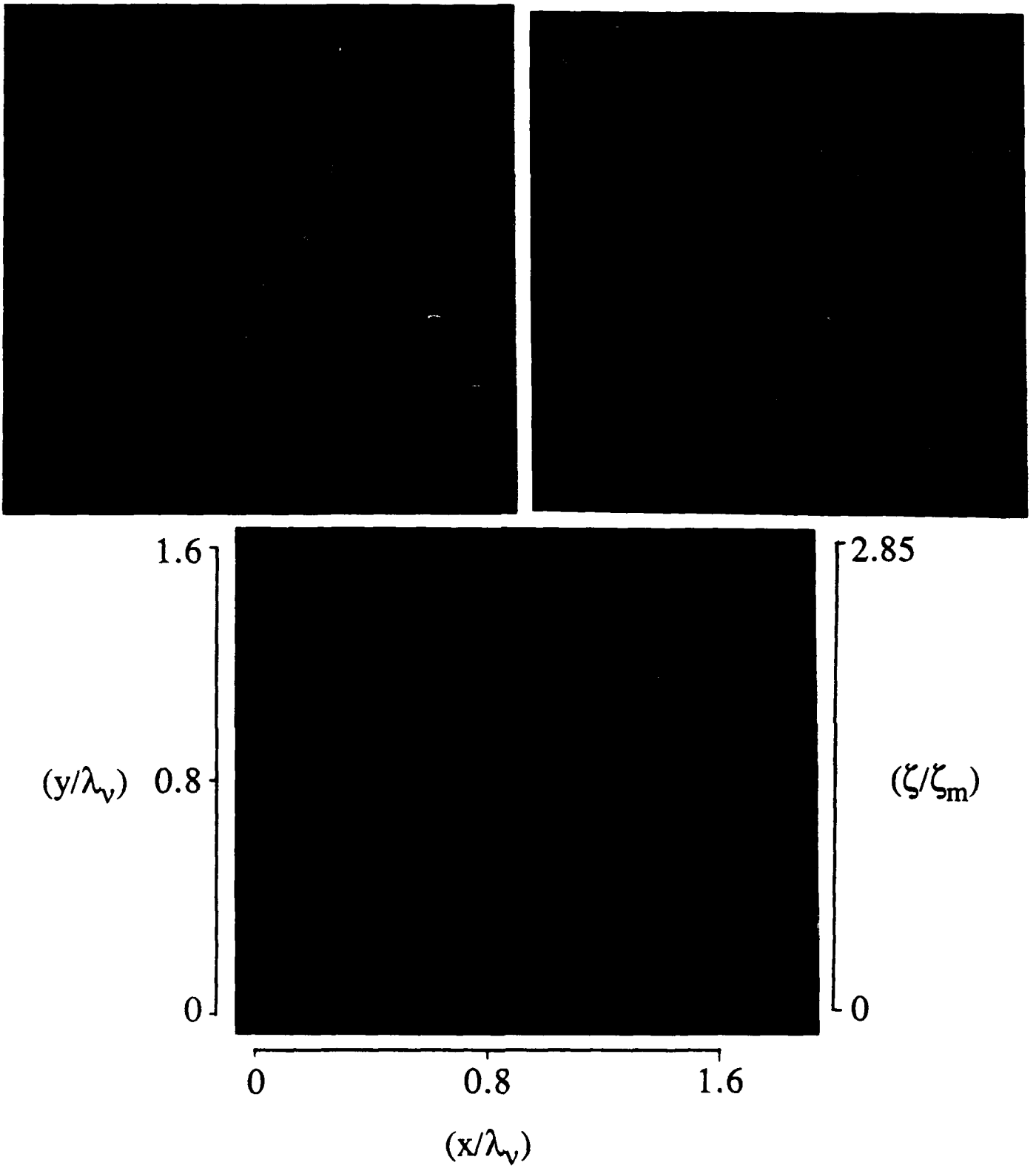

Fig. 4. The measured Sc » 1 conserved scalar field $\zeta(x,t)$ in three typical successive 256 × 256 spatial data planes. The 256 different colors denote the local conserved scalar value at each data point. The x-axis points to the right, the y-axis points up, and the z-axis points out of the page. The three planes are shown in order of increasing z (and therefore increasing t) in the clockwise direction, beginning at the upper left. Each data plane spans approximately $^1/_{17}$ of the local outer scale δ in Fig. 1, or approximately 1.6 times the local inner scale λ_v, in both directions. The true scalar energy dissipation rate field obtained by differentiation of these data in all three directions is shown in Fig. 5.

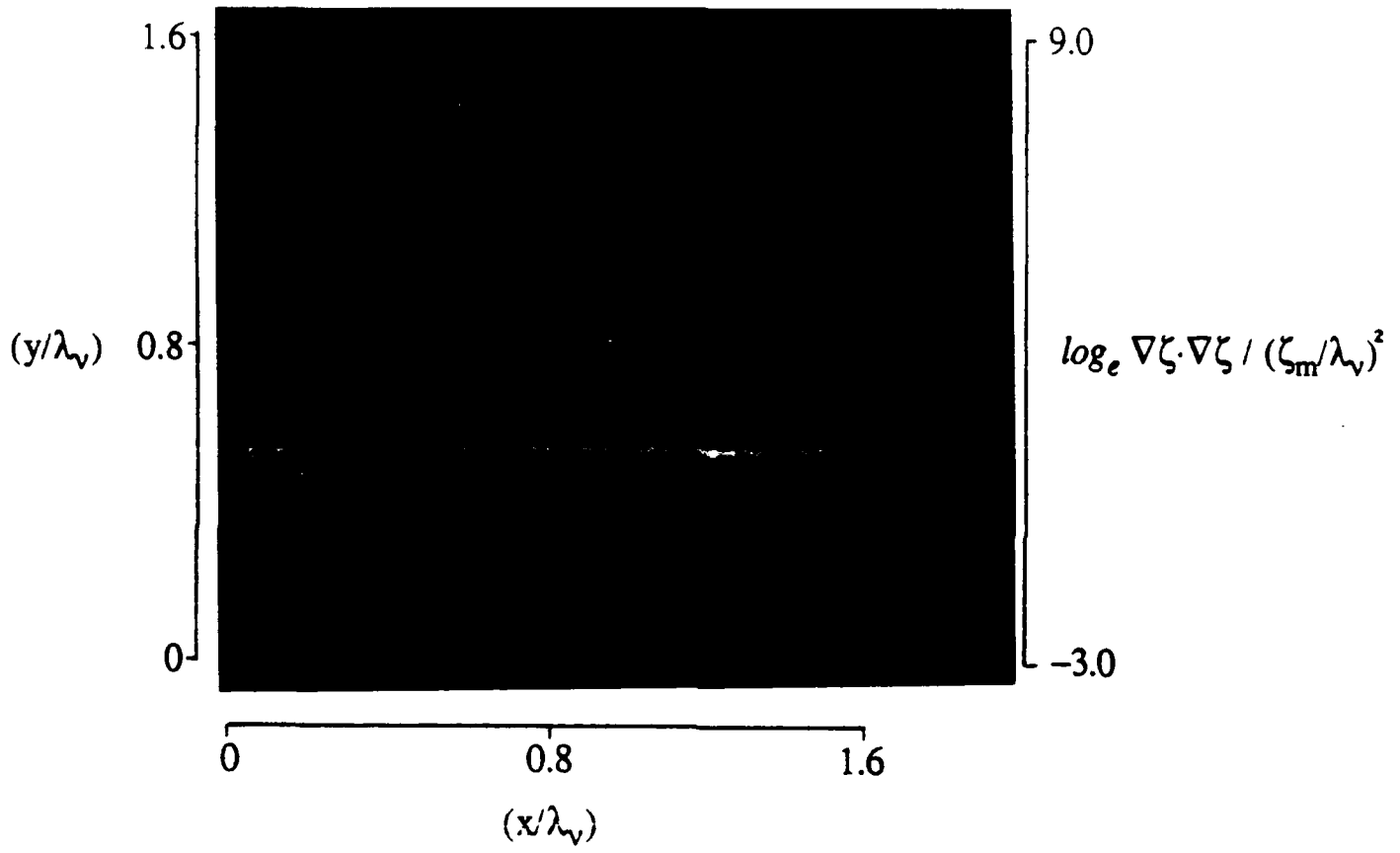

Fig. 5. The logarithm of the scalar energy dissipation rate field $log_e \nabla\zeta\cdot\nabla\zeta(x,t)$ in a typical spatial data plane, obtained by direct differentiation of the conserved scalar data in the three adjacent data planes shown in Fig. 4 using linear central differences. The 256 different colors give the logarithm of the local instantaneous mixing rate in the flow Note the fine structure of the molecular mixing process as a collection of sheet-like strained molecular diffusion layers. The time evolution of the dissipation field in this spatial data plane is shown in Fig. 6.

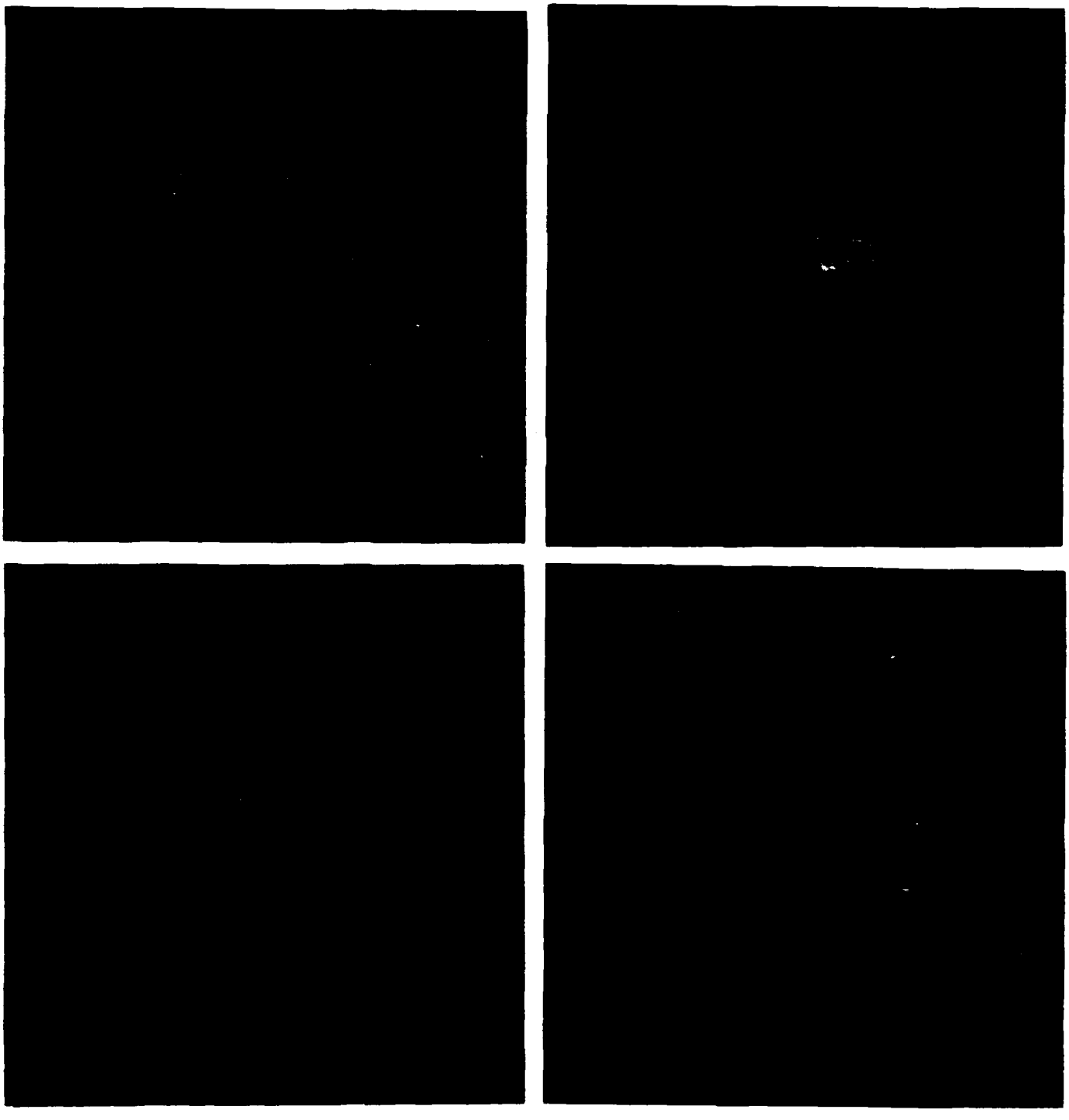

Fig. 6. The time evolution of the scalar energy dissipation rate field $log_e \nabla\zeta \cdot \nabla\zeta(x,t)$ in a typical data plane from four temporally successive three-dimensional spatial data volumes (see Fig. 2). Time increases in the clockwise direction beginning at the upper left. Note that the resulting ΔT is slightly less than 1/2 (λ_D/u).

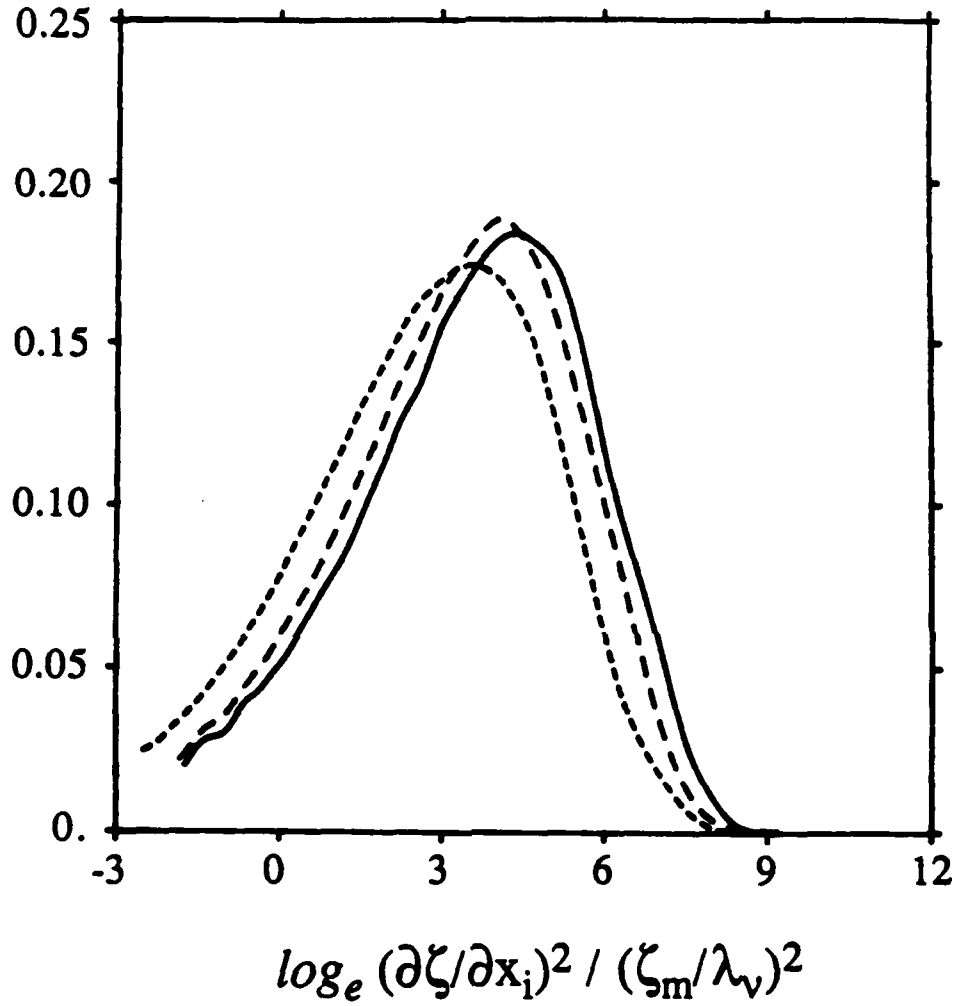

Fig. 7. **Probability densities for the logarithm of the square of each of the three vector components of $\nabla\zeta(x,t)$ as a check on the anisotropy of the scalar field within the four-dimensional data space.**

——— $(\partial\zeta/\partial x)^2$; – – – – $(\partial\zeta/\partial y)^2$; - - - - - $(\partial\zeta/\partial z)^2$.

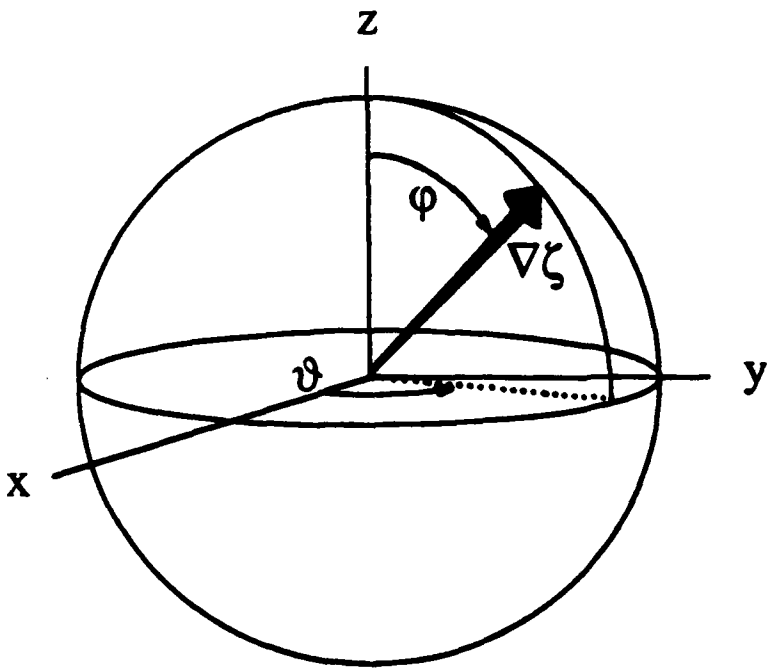

Fig. 8. The spherical orientation angles ϑ and φ of the scalar gradient vector $\nabla\zeta(\mathbf{x},t)$ relative to the x-y-z coordinate axes in Fig. 4-6.

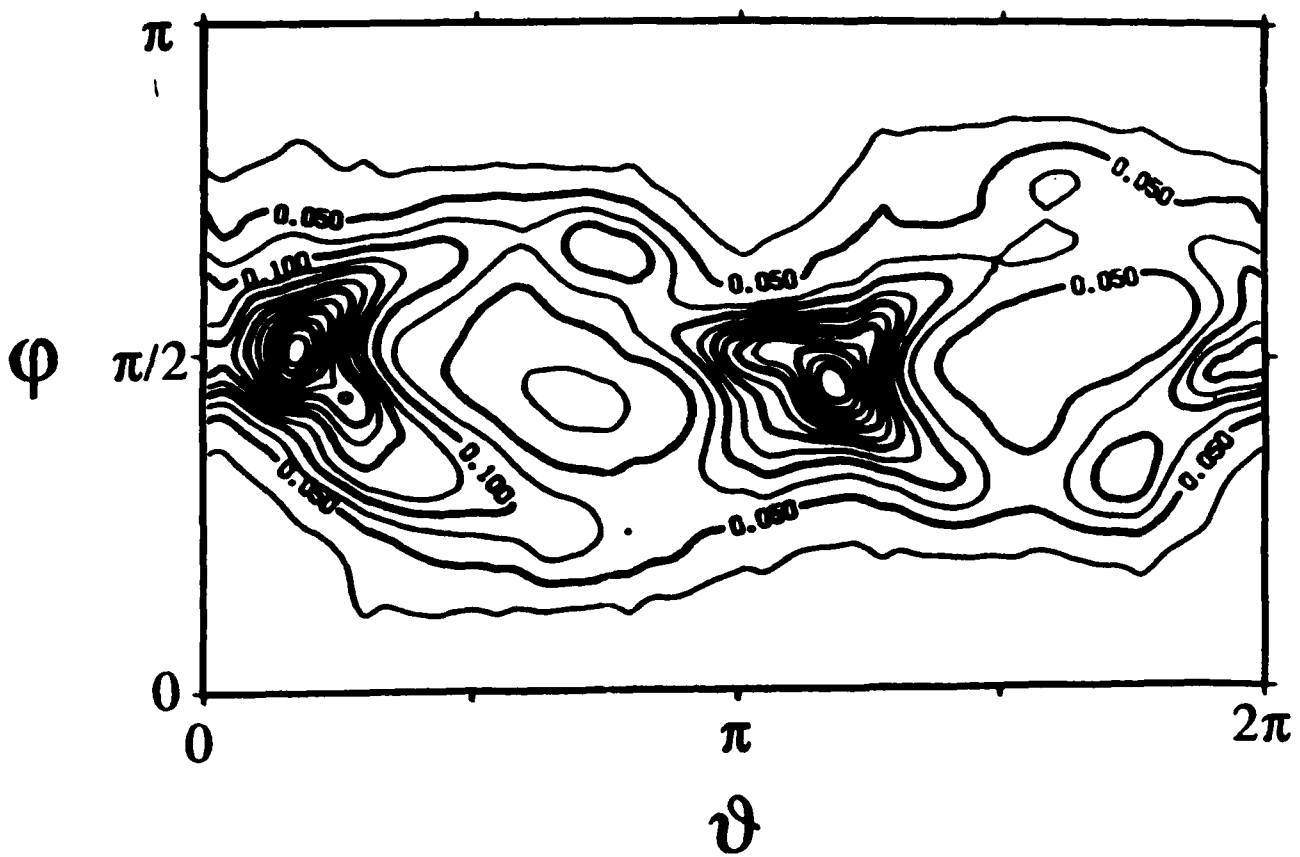

Fig. 9. The joint probability density $\beta(\vartheta,\varphi)$ of spherical orientation angles for the scalar gradient vector field $\nabla\zeta(x,t)$ obtained from the present measurements.

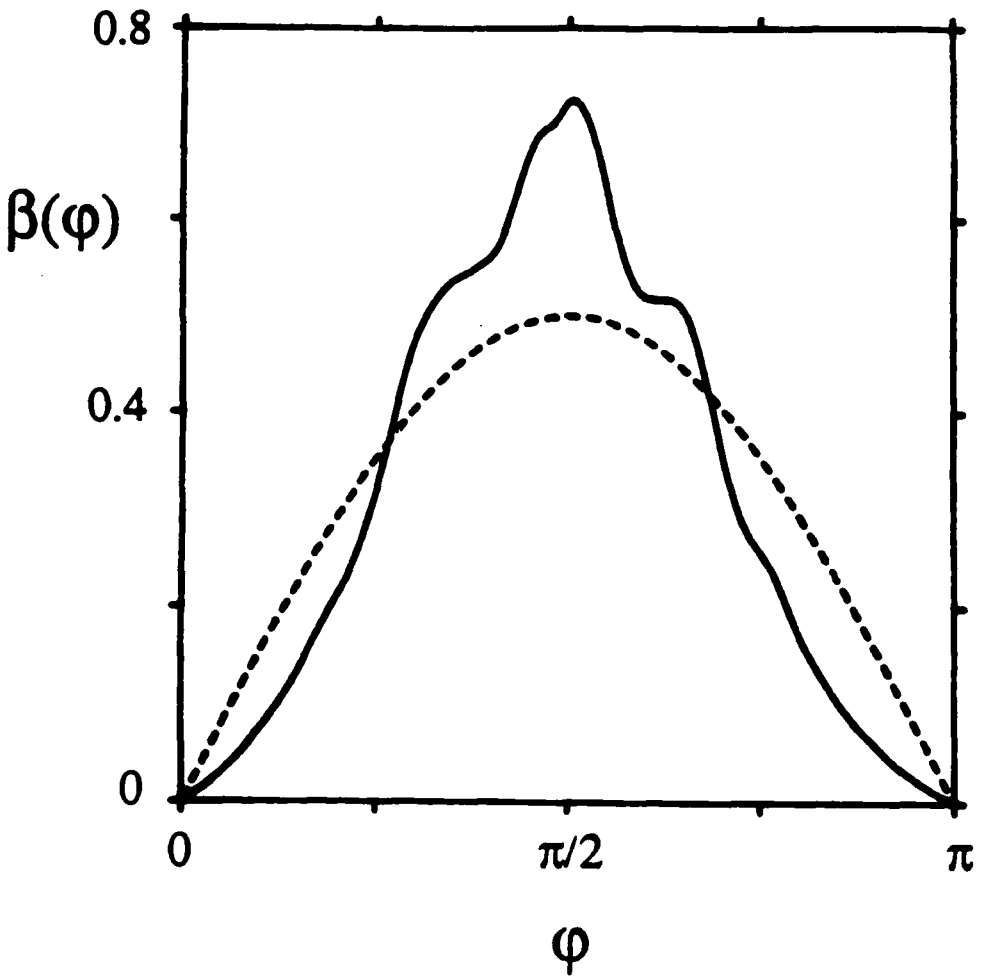

Fig. 10. The individual probability densities of spherical orientation angles for the scalar gradient vector field. (a) $\beta(\varphi)$ giving orientation relative to the z-axis. (b) $\beta(\vartheta)$ giving orientation of the gradient vector projection into the x-y plane.

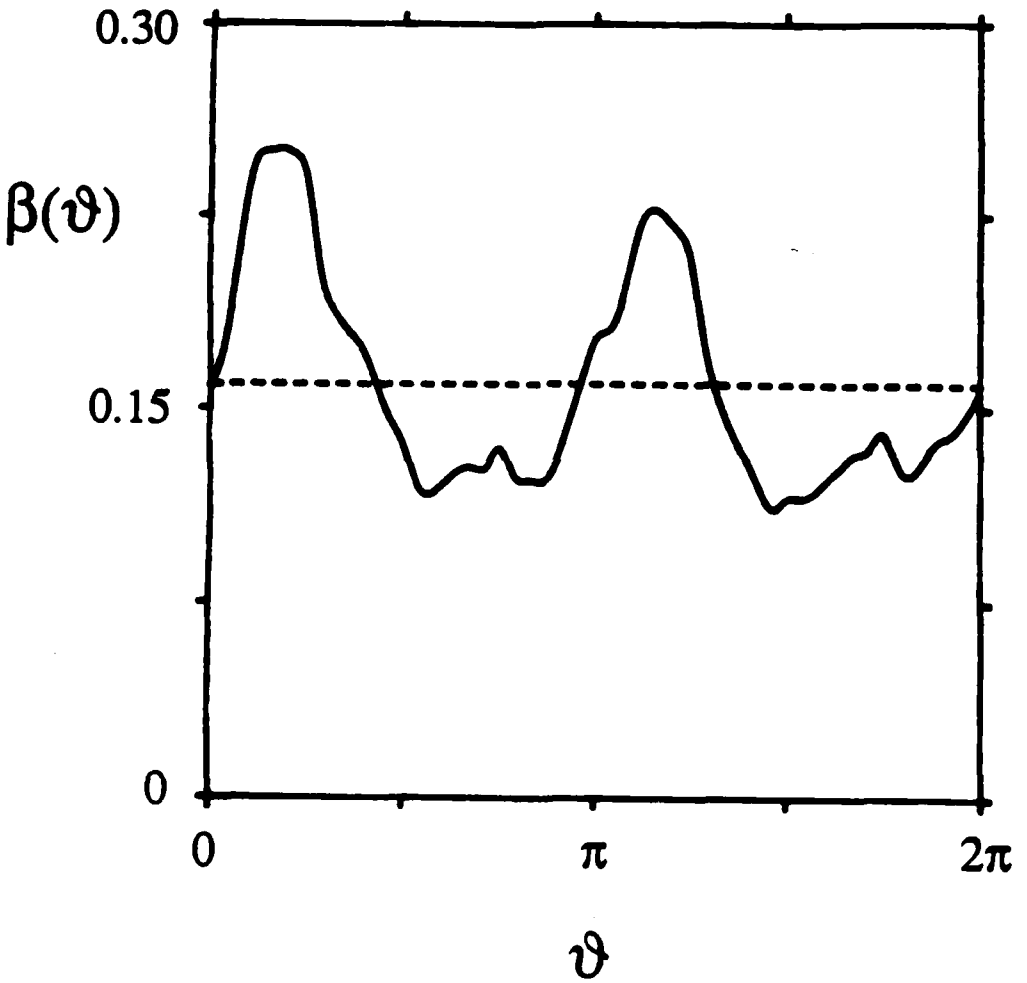
0.30
β(ϑ)
0.15
0
0
π
2π
ϑ

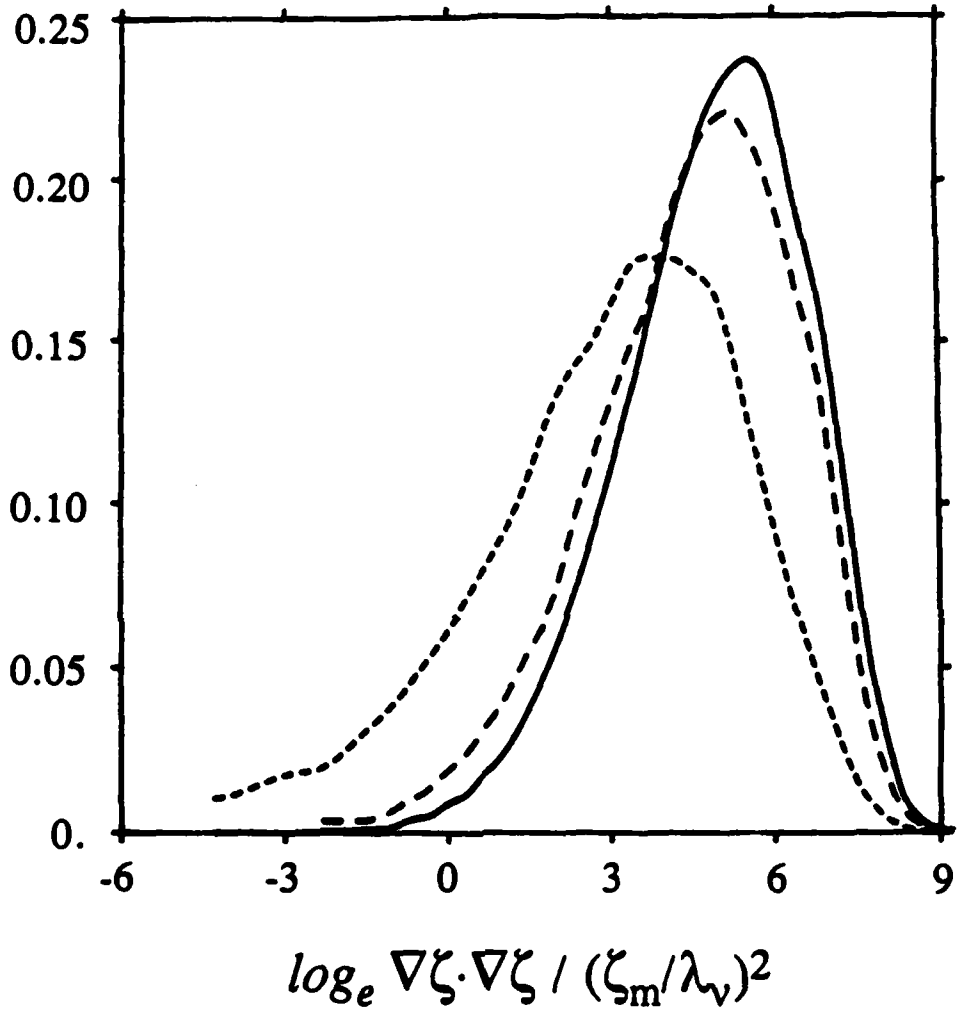

Fig. 11. The distribution of mixing rates obtained from one- and two-dimensional approximations of the scalar dissipation $\nabla\zeta\cdot\nabla\zeta(x,t)$, compared with the result obtained from all three components of the gradient field.

- - - - - $(\partial\zeta/\partial x)^2$; – – – – $(\partial\zeta/\partial x)^2 + (\partial\zeta/\partial y)^2$; ——— $(\partial\zeta/\partial x)^2 + (\partial\zeta/\partial y)^2 + (\partial\zeta/\partial z)^2$.

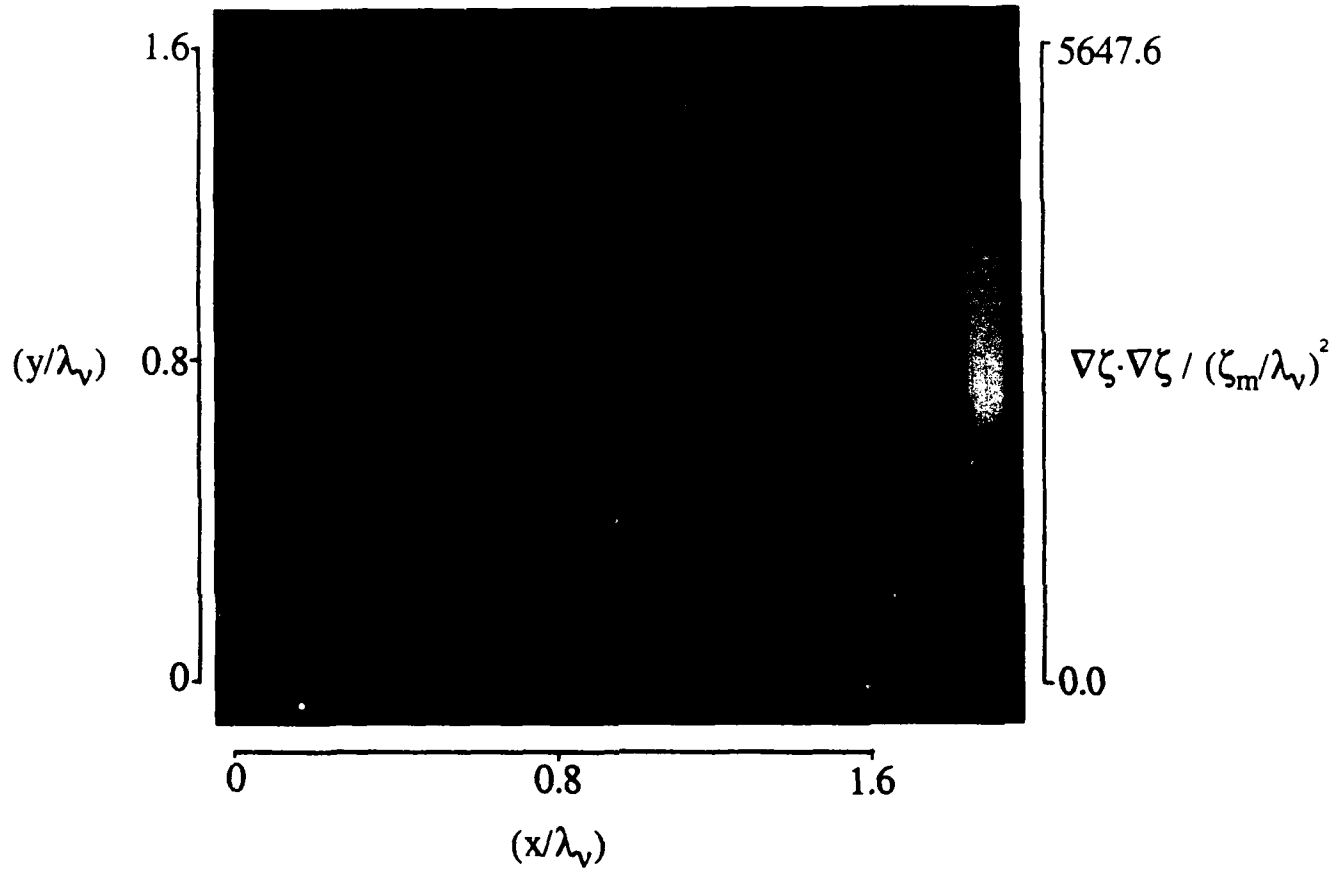

Fig. 12. The scalar energy dissipation rate field $\nabla\zeta\cdot\nabla\zeta(\mathbf{x},t)$ in the same data plane shown logarithmically in Fig. 5. Colors from blue to red denote linearly increasing dissipation rates. Note that only very little of the flow contains high dissipation rates, indicating the 'spottiness' of the dissipation field.

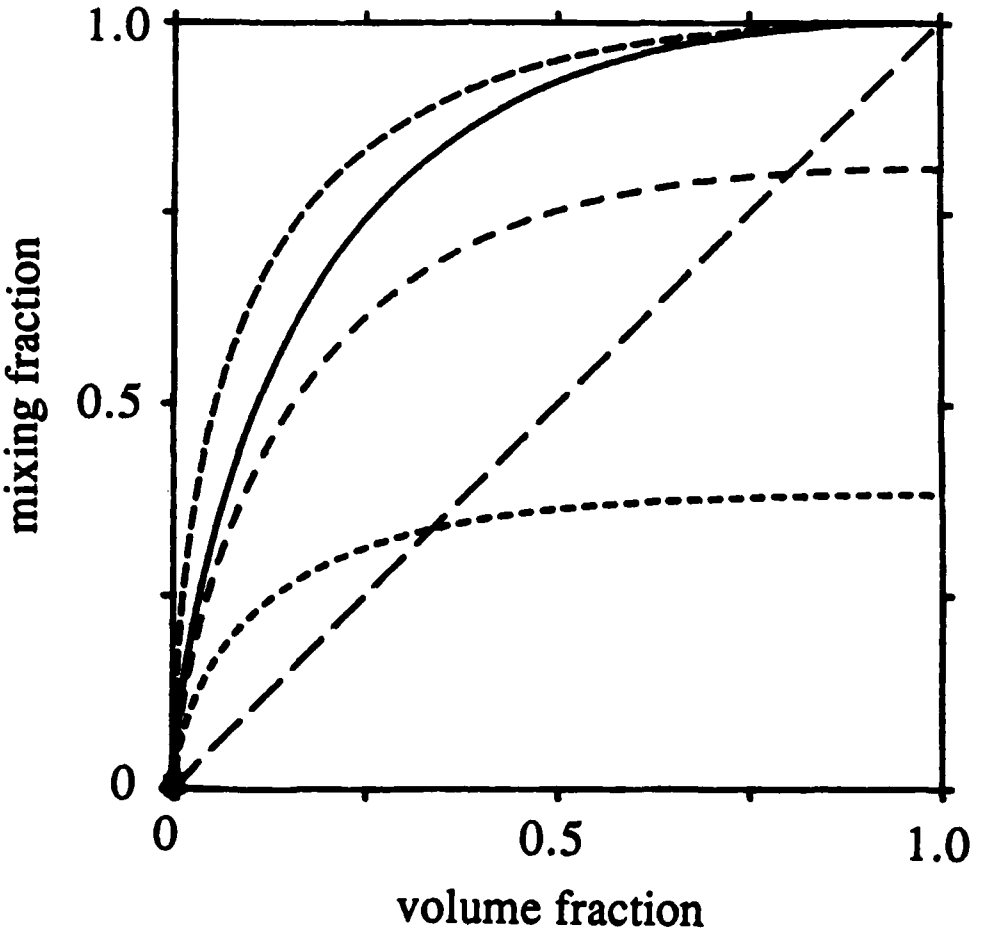

Fig. 13. The fraction of the total mixing achieved by the flow versus the fraction of the total volume within which the mixing occurs, quantifying the 'spottiness' of the scalar dissipation field. Note, for example, that nearly 10% of the mixing is achieved in just 1% of the volume, 50% of the mixing is accomplished in slightly less than 12% of the volume, and 90% of the mixing occurs in just over 45% of the volume. Also shown are the results obtained from lower-dimensional approximations of the dissipation field.

——— Present 3D result; - - - - 2D approximation; ..... 1D approximation; - - - - - lognormal result; — — — homogeneous result.

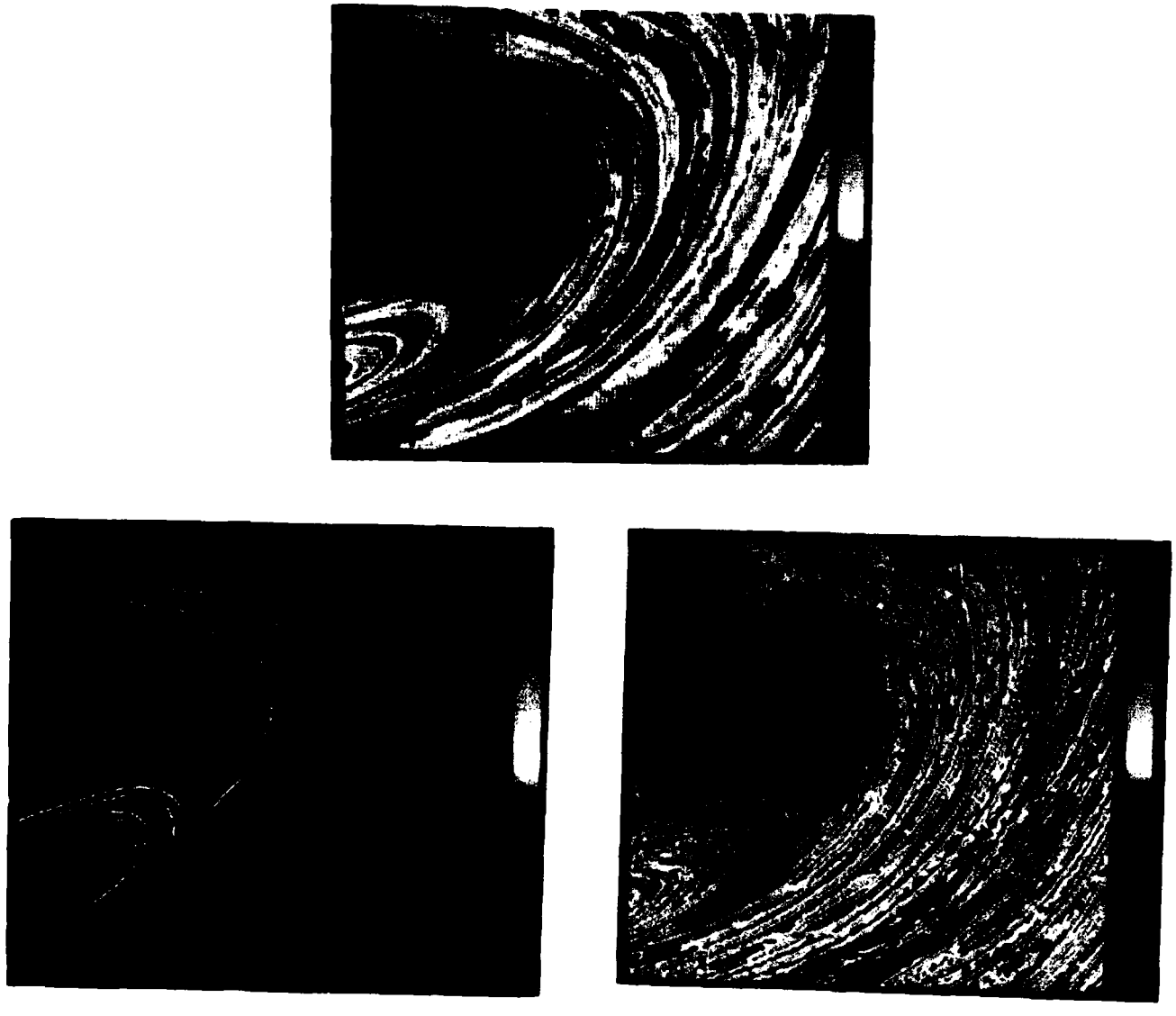

Fig. 14. Present digitizations and processing of scalar field $\zeta(\mathbf{x},t)$, scalar dissipation field $\nabla\zeta\cdot\nabla\zeta(\mathbf{x},t)$, and $log_e\nabla\zeta\cdot\nabla\zeta(\mathbf{x},t)$ from low Reynolds number chaotic advection experiments of Ottino (1989), revealing fine scale structure of the scalar dissipation field as isolated and interacting strained laminar diffusion layers similar to those seen from our turbulent flow measurements.

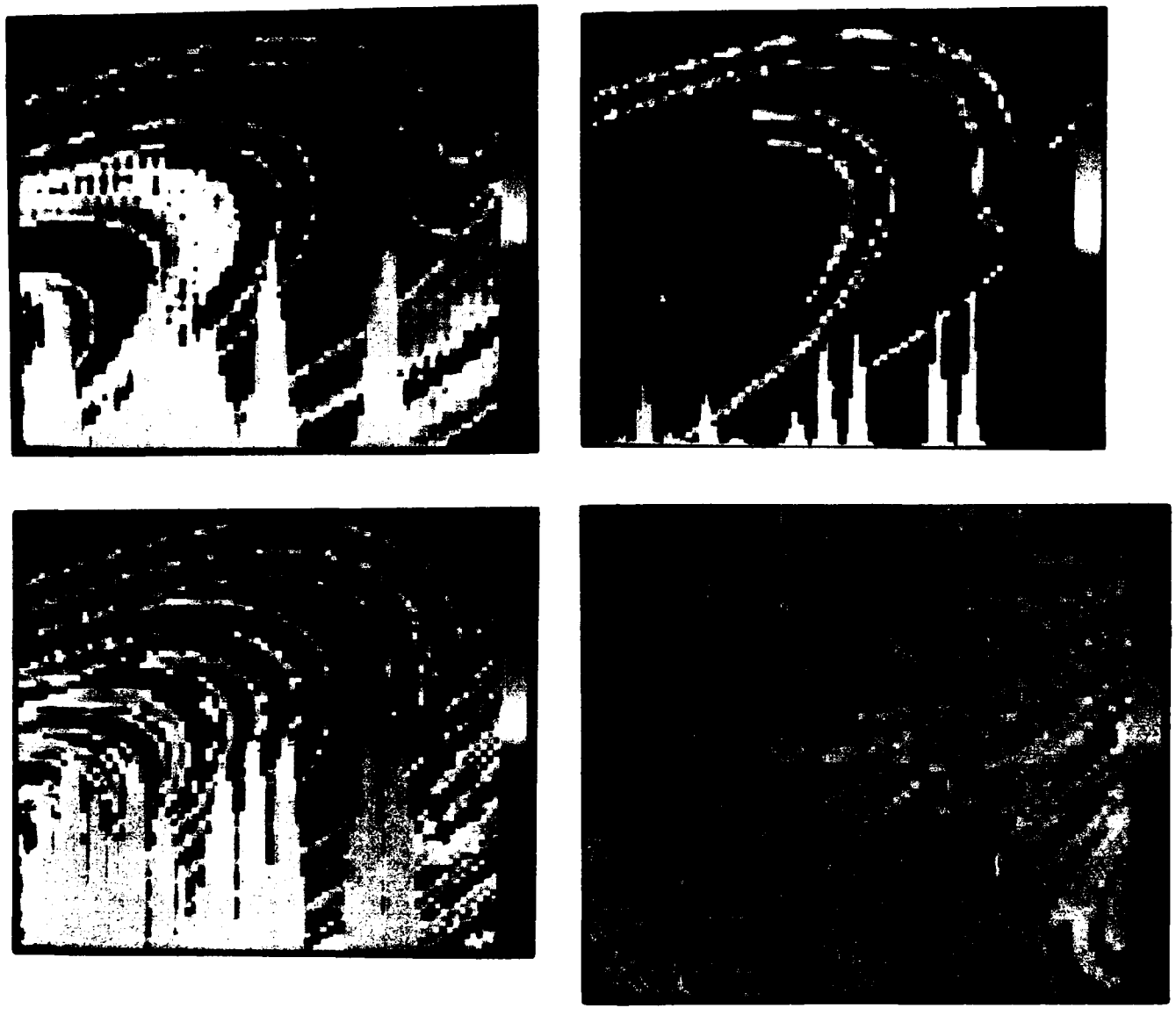

Fig. 15. Zoomed-in views of the scalar field $\zeta(\mathbf{x},t)$, the scalar dissipation field $\nabla\zeta\cdot\nabla\zeta(\mathbf{x},t)$, and the logarithm of the disipation field $log_e\nabla\zeta\cdot\nabla\zeta(\mathbf{x},t)$ from the low Re chaotic advection flow in Fig. 14 and the corresponding $log_e\nabla\zeta\cdot\nabla\zeta(\mathbf{x},t)$ from our turbulent flow measurements (lower right), showing profiles slicing through each field. Note the similarity in the overall structure of the dissipation fields as well as the internal structure of the diffusion layers in both the low Re chaotic flow and the turbulent flow (see §3.5).

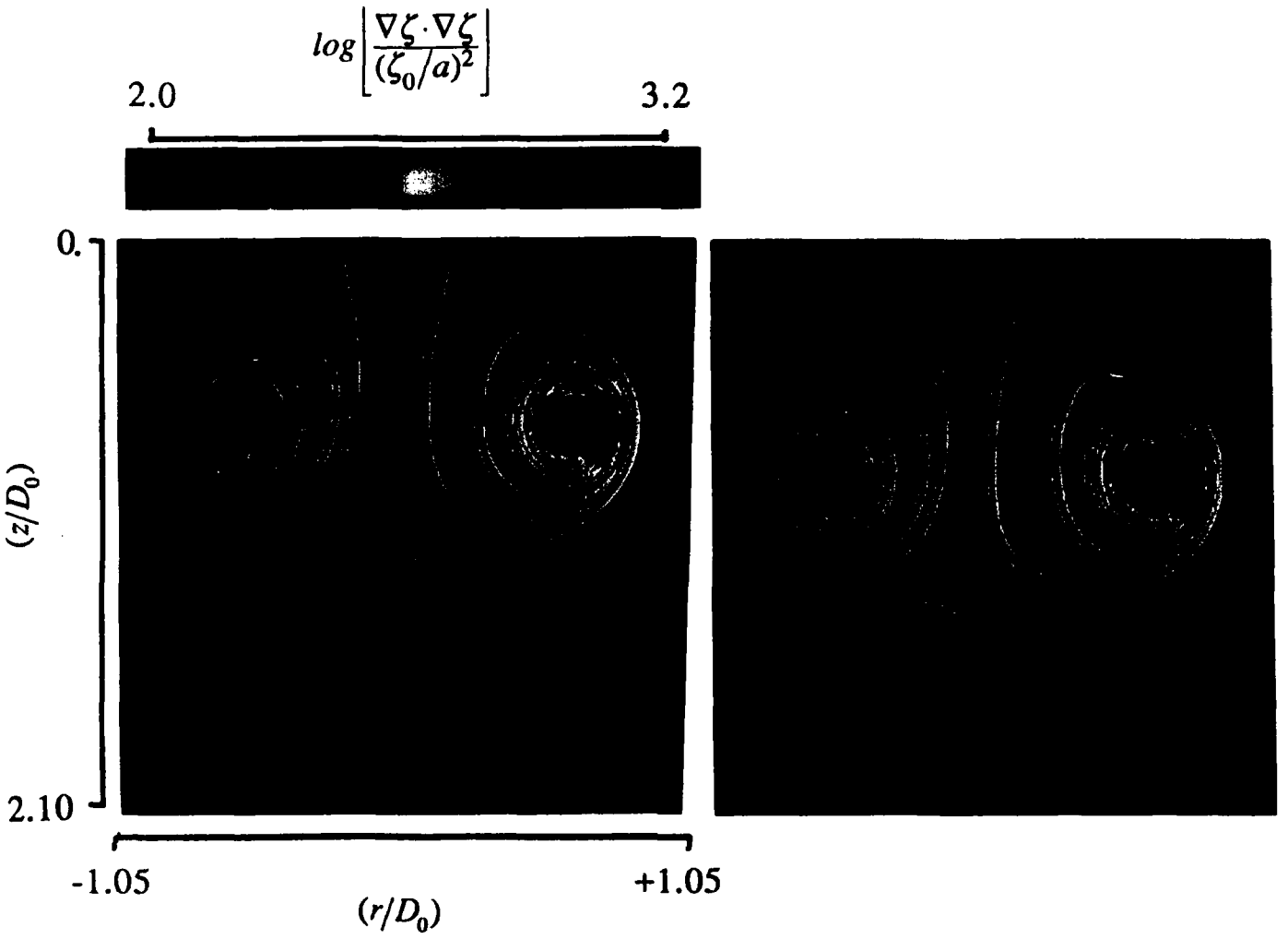
$log\left|\frac{\nabla\zeta\cdot\nabla\zeta}{(\zeta_0/a)^2}\right|$
2.0
3.2
0.
2.10
(z/D_0)
-1.05
+1.05
(r/D_0)

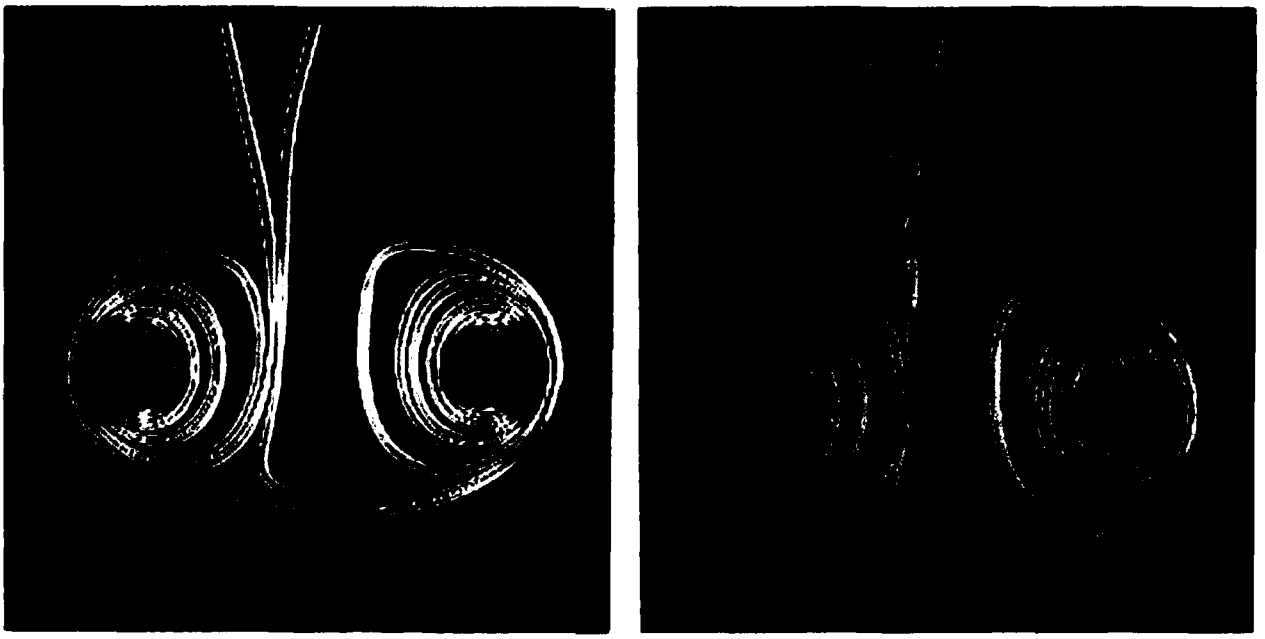

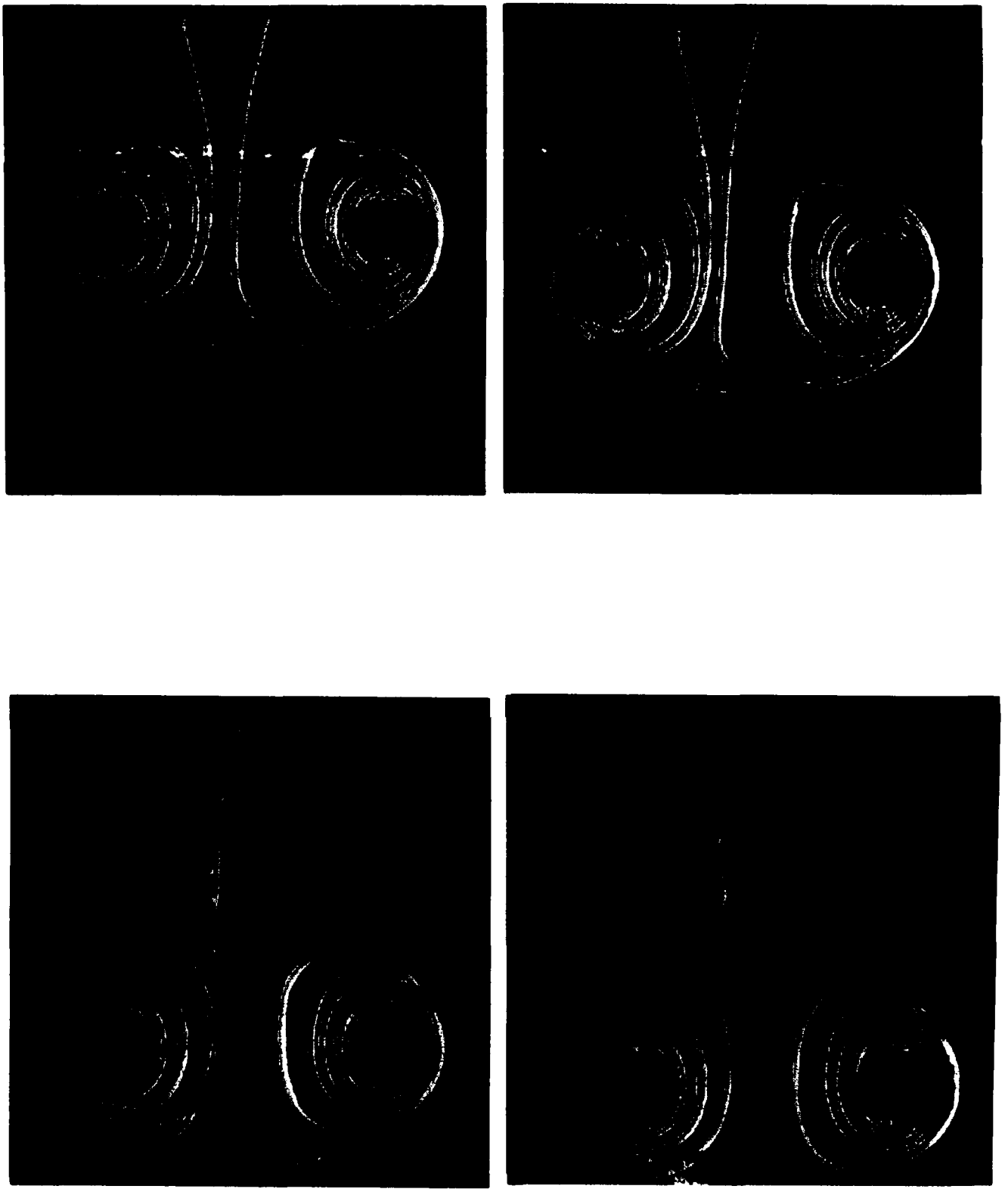

Fig. 16. The logarithm of the dissipation rate field $log_e \nabla\zeta\cdot\nabla\zeta(x,t)$ during the pinch off phase of a laminar vortex ring. The dimensionless time between successive panels shown is $(\Delta t\cdot\Gamma/2\pi a^2) \approx 0.089$. Note in particular the diffusional cancellation occurring between the two molecular diffusion layers emanating from the nozzle lip (see §3.6), as well as the similarity between the dissipation layers seen here and the vorticity layers in this flow. (See Eqs. (6) and (7) and related discussion in §3.6).

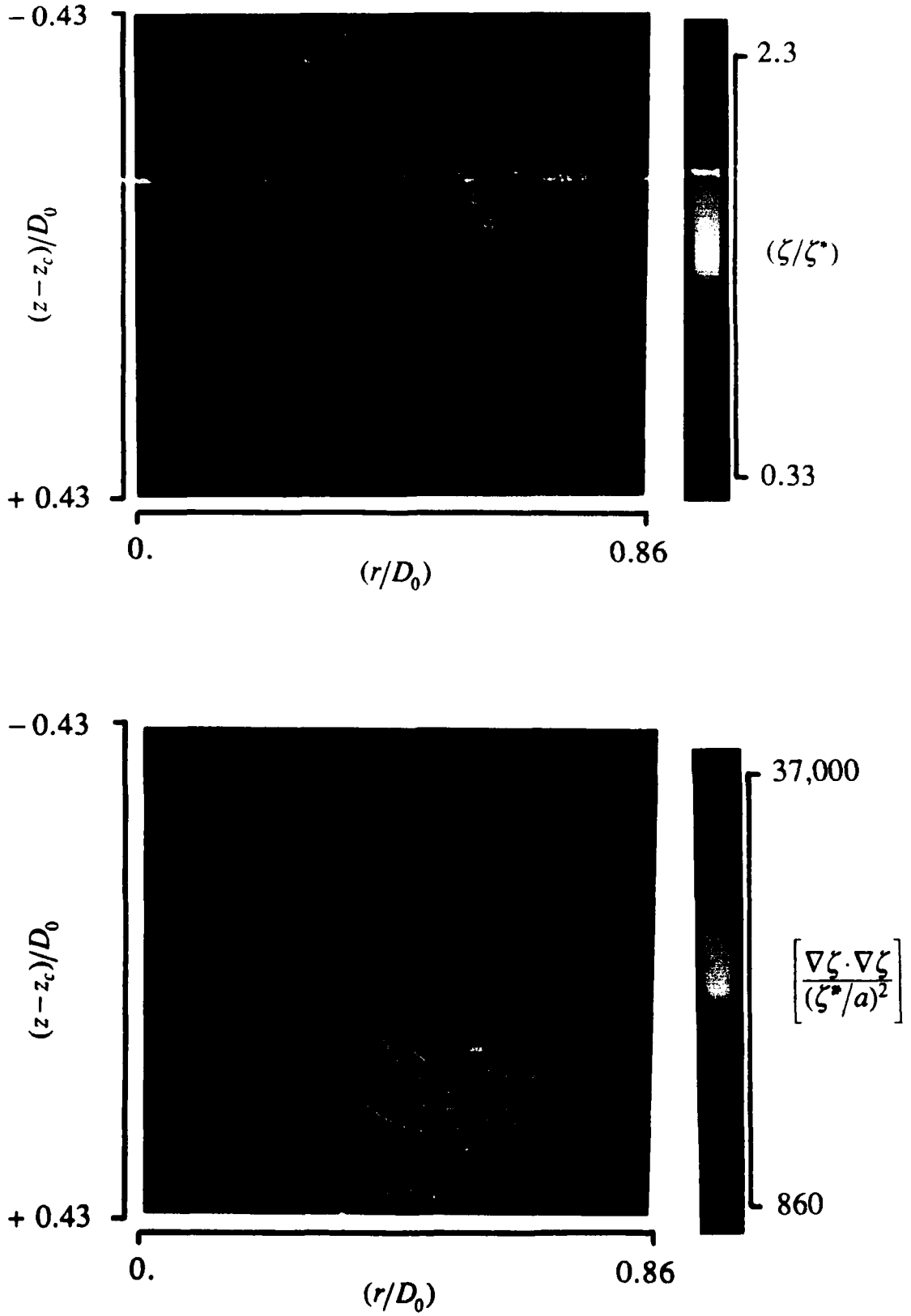

Fig. 17. Present measurements of the asymptotic structure of the laminar vortex ring, showing right half of the ring only. *(a)* The scalar field $\zeta(\mathbf{x},t)$. *(b)* The scalar dissipation rate field $\nabla\zeta\cdot\nabla\zeta(\mathbf{x},t)$. Note the diffusional cancellation occurring among the molecular diffusion layers near the core of the ring.

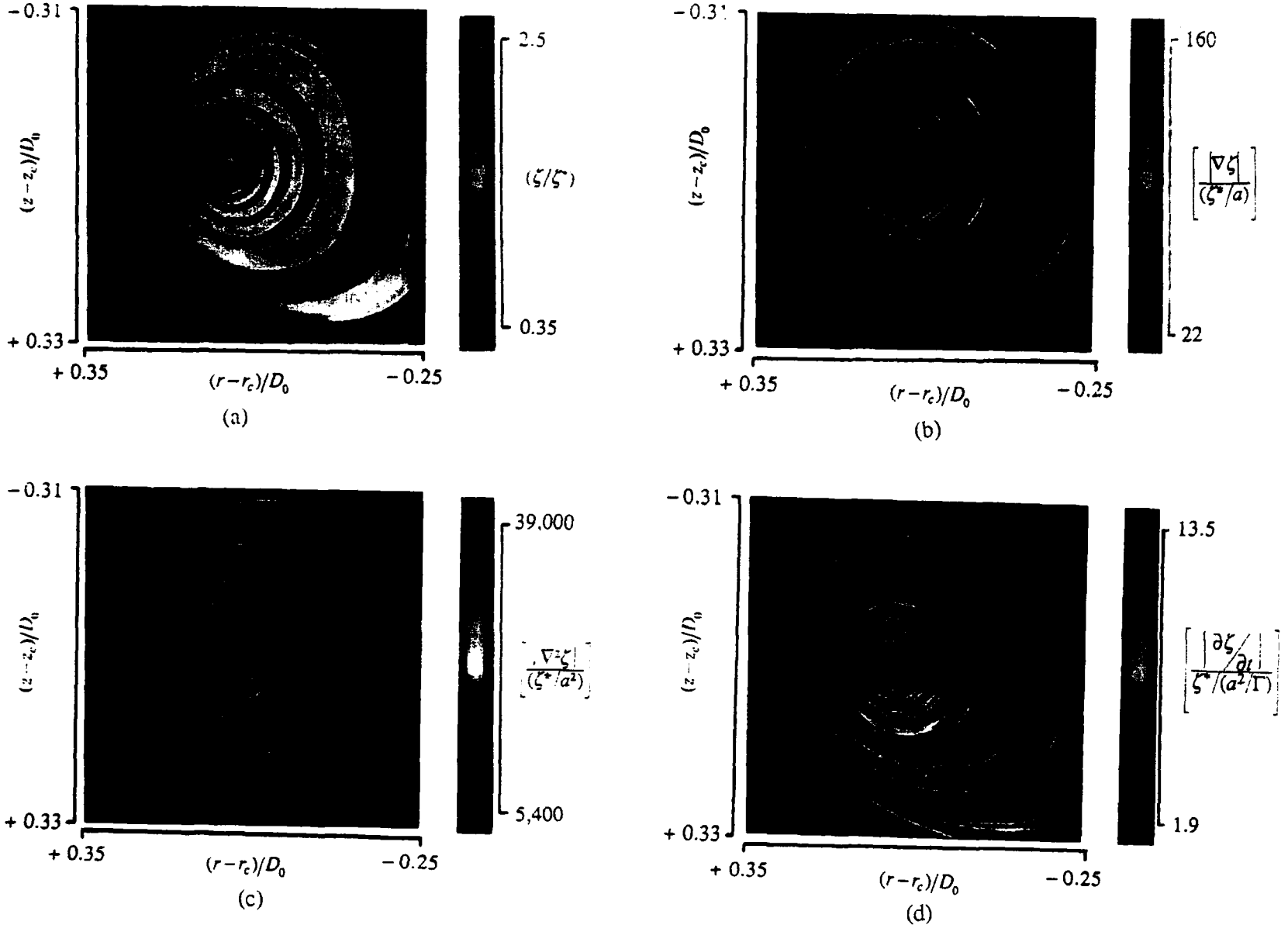

Fig. 18. The component fields involved in inverting the mixing process described by Eq. (1) to obtain the velocity component field $u_{||}(\mathbf{x},t)$. (a) The original scalar field measurement $\zeta(\mathbf{x},t)$. (b) The resulting gradient magnitude field $|\nabla\zeta(\mathbf{x},t)|$. (c) The resulting Laplacian field $\nabla^2\zeta(\mathbf{x},t)$. (d) The time derivative field $\partial\zeta(\mathbf{x},t)/\partial t$. (See related discussion in §3.7.)

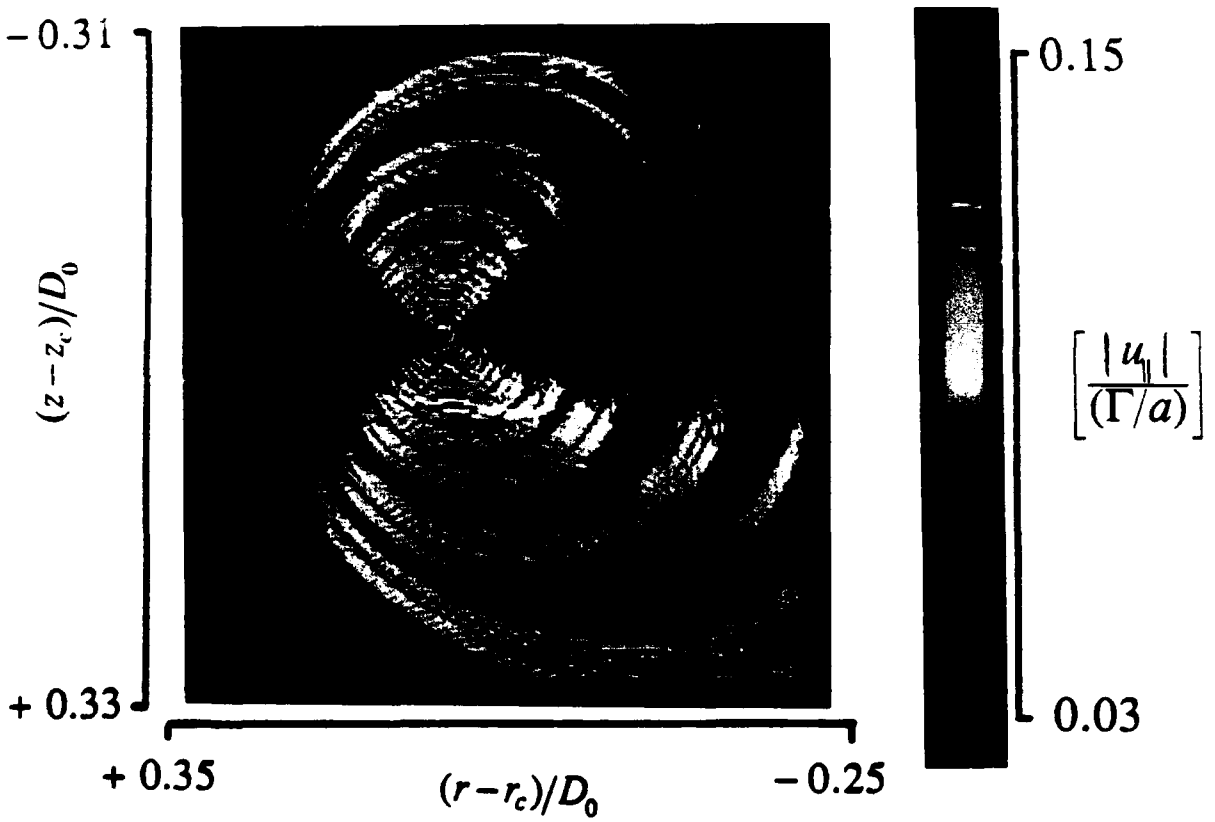

Fig. 19. The velocity component along the local scalar gradient vector direction, $u_{\|}(\mathbf{x},t)$, obtained via the scalar imaging velocimetry technique (SIV) from the component fields in Fig. 18.